Chapter 6

Computational Tools for Nitroxide Design

Nicholas S. Hill, Benjamin B. Noble, Fergus J. M. Rogers, Alfred K. K. Fung and Michelle L. Coote*

ARC Centre of Excellence for Electromaterials Science, Research School of Chemistry, Australian National University, Canberra ACT 2601, Australia

*Corresponding author: michelle.coote@anu.edu.au

Table of Contents

Abstract

Computational tools for modelling nitroxide radical chemistry are outlined and illustrated through a series of case studies. Different types of application raise different problems. Herein we outline and assess the computational methods available for modelling high spin systems, predicting EPR hyperfine coupling constants, redox potentials, alkoxyamine dissociation equilibria and photochemical processes. While high spin systems and excited states are best modelled with complex multi-reference methods incorporating static and dynamic correlation, there is a growing family of more economical approaches that can often achieve an acceptable level of accuracy. Redox potentials and alkoxyamine dissociation equilibria require only single reference methods, albeit at a high level of theory, but the accurate treatment of solvation remains an ongoing challenge. Modelling EPR requires a range specialist techniques and basis sets to accurately capture core correlation. Through the case studies presented here we not only show that accurate and useful quantitative predictions are possible, but introduce a wide range of complementary tools for enhancing our qualitative understanding of structure-reactivity trends.

6.1 Introduction

Nitroxides are a class of molecules that exhibit a wide range of chemical properties, the most significant and useful of which is their stability as radical species. This radical stability has been utilised for a wide range of chemical applications, including nitroxide-mediated polymerisations, as fluorescent probes, and in electron paramagnetic resonance spectroscopy. They are also able to undergo reversible oxidation and reduction, which has been harnessed in batteries, solar cells, synthesis and even as medicinal antioxidants. The many and various properties of nitroxides and their applications have been explored throughout this book; this chapter will focus primarily on the methods and considerations for simulating their properties and reactivity.

Computational chemistry is becoming an increasingly powerful tool for modern chemists, as require theoretical insights are often invaluable when rationalising experimental results. Throughout the chapter, emphasis has been placed on utilising modern methods, software packages, and literature references to provide an up-to-date overview of how a new computational chemist may begin to tackle the challenges of nitroxide chemistry. Many of the computational lessons taught in this chapter are generally applicable to other areas of organic chemistry; the challenge often with nitroxides is that many of their properties that may be otherwise calculated in isolation are often coupled, for example combining nitroxide-mediated polymerisations (NMP), with their dependence on accurate kinetic parameters, with photochemistry, and the difficulties when modelling excited states, is necessary to study photo-NMP.

To that end, for type of model chemistry, different theoretical considerations are explored, such as single- vs multi-reference and combinations thereof, and the impact of different basis sets. Quantitative and qualitative results are also discussed throughout, as are the ability for different approaches to achieve them, and wherever possible recommendations are made. We start with a discussion of the methods needed to model complex spin systems, for which the challenge is the accurate treatment of static correlation without incurring the massive costs of extensive multi-reference calculations. We then examine the methods needed to simulate EPR spectra, which among other things requires specialised basis sets for the correct treatment of core correlation. We then turn to redox chemistry, where the focus shifts to the high-level single reference methods methods needed for treating dynamic correlation. For redox chemistry in particular, the treatment of solvent effects also becomes a major potential source of error, due to the participation of charged species. We then examine alkoxyamine dissociation in the context of nitroxide mediated polymerization, which uses similar methods to redox chemistry but quite different strategies in structure-reactivity analysis. Finally, we examine methods for the treatment of excited states, particularly in the context of photo-NMP.

6.2 Modelling Complex Spin Systems

Many problems of interest are not adequately handled by conventional methods. Important examples involving nitroxides can be found in transition metal complexes, polyradicals, many excited-states, as well as the intermediate structures encountered in bond-dissociation events.[1-5] These cases are said to be “strongly correlated”, meaning that methods based on a *single reference* wavefunction are a poor approximation of the exact solution. Numerous strategies for dealing with these problems are nonetheless available to the modern chemist,

but the functionality is often peculiar and system dependent. We discuss the general theory supported by some recent applications here.

6.2.1 Dynamic versus Static Correlation Energy

Quantum-chemical methods differ in their accuracy and complexity primarily through their approaches to modelling the correlation energy (E_c). In the crudest sense, correlation is the error arising from the Hartree-Fock (HF) approximation to the exact, non-relativistic, time-independent Schrodinger equation within the Born-Oppenheimer approximation:[6, 7]

$$E_c = E - E_0 \qquad (1)$$

where E is the *exact* energy of the system, and E_0 is the energy of the corresponding (HF) wavefunction. Correlation has a somewhat different definition in density functional theory (DFT), however the implications are similar.[8]

In the HF regime, the many-body wavefunction is reduced to a Slater determinant $|\Psi\rangle$ of one-electron molecular spin-orbitals (MO). Each MO is "independent", experiencing only the average field generated by all the electrons in the system, such that the explicit many-body nature of the problem is substituted for a coupled set of soluble one-body problems. Indeed, it is from this model that we derive the familiar MO conception of molecular electronic structure.

The ground-state solution to the resultant set of HF equations provides an *upper-bound* to the exact ground-state energy such that the error, E_c, is always negative; although this is not necessarily true of the excited states. In general, the complex MOs cannot not be determined analytically, so a finite *basis set* of N *basis functions* or atomic orbitals (AO) is introduced, and the MOs are expanded in terms of these. Since the HF equations are nonlinear, the AOs are iteratively mixed together to construct the lowest energy set of N MOs (the self-consistent field method) such that, for an M electron HF system, M MOs are completely occupied and $N - M$ are empty or *virtual*. In this sense HF is a single-reference approximation, as a Slater determinant is evidently based on only one "configuration" of occupied MOs.

Correlation energy can be systematically recovered by expanding the total ground-state wavefunction $|\Phi_0\rangle$, as a linear combination of the HF reference $|\Psi_0\rangle$, and its "excited" configurations (configuration interaction or CI):

$$|\Phi_0\rangle = c_0|\Psi_0\rangle + \sum_{i>a}^{m} c_a^i|\Psi_a^i\rangle + \sum_{i,j>a,b}^{m} c_{a,b}^{i,j}|\Psi_{a,b}^{i,j}\rangle + \cdots \qquad (2)$$

where and $|\Psi_i^a\rangle$, $|\Psi_{i,j}^{a,b}\rangle$ are the singly and doubly excited determinants formed by elevating electrons from occupied (i, j *etc*.) to virtual HF MOs (a, b *etc*.). The expansion coefficients c_n, are determined from the CI matrix– an eigenvalue problem – whose solutions correspond to the ground- and excited-states of the system. In the full CI (FCI) limit, where all possible excitations are considered, the exact correlation energy is recovered completely within the bounds of the basis set. Such a calculation is virtually unfeasible however, as the number of determinants in the CI expansion has factorial dependence on the number of AOs. In practical applications, E_c is instead approximated by truncating the expansion or more commonly, by applying perturbation, coupled pair or Green's function theory. For the interested reader, archetypal methods are discussed in Chapter 4 onwards of Ref [6].

Single-reference post-HF and DFT methods deal directly with so-called dynamical correlation, *i.e.* the error relating to electronic motion. Static correlation, the focus of this section, arises from errors due to the use of a single reference wavefunction, and occurs when there is more than one dominant resonance contributor.[9] A simple but illustrative example is the σ-bond dissociation problem. At the equilibrium geometry, the HF reference consisting of the σ^2 configuration, is physically sensible. As the bond is stretched however, the $(\sigma^*)^2$ configuration becomes increasingly important such that at the dissociation limit, both configurations have equal weight in the ground-state wavefunction. In this case, at least two MO configurations are necessary for a valid description of σ-bond dissociation.

INSERT FIGURE 6.1

Unlike dynamical correlation, static correlation is recovered only slowly by expansions of the type in equation (2). Efficient treatment of statically correlated problems therefore requires instead a more general reference than the single-reference wavefunction. Such a wavefunction can be found in the multireference framework, *i.e.* where the reference is a superposition of two or more MO configurations. In the multi-configurational self-consistent field (MCSCF) method, the multireference generalisation of SCF, MOs and CI coefficients are varied simultaneously in solving for a particular state. In this way, MCSCF could be thought of as the union of HF, where only MOs of a single determinant are varied, and CI, where the expansion coefficients are varied within in a basis set of frozen MOs.[10]

6.2.2 Multireference Methods.

MCSCF is most commonly encountered in two related formalisms, namely the complete active space self-consistent field (CASSCF) method, and its reduced analogue, restricted active space self-Consistent field (RASSCF). In both schemes, the determinants defined for MCSCF are generated by a full CI treatment of an *active space*, a selection of orbitals generated by an initial HF calculation.[11] CASSCF considers every configuration of the expansion, whilst RASSCF invokes a set of selection criterion to reduce the number of configurations to only the most pursuant contributors. These specifications are denoted $[n, m]$-RAS/CASSCF or RAS/CAS(n, m), where n and m are the number of active space electrons and orbitals respectively.

The resultant set of configurations grows aggressively with the size of the active space, so the practical challenge occurs in selecting a computable specification which best represents the chemistry of the problem. As a minimum, this must include all MOs that are expected to change significantly during some transformation, as well as those which are partially occupied.[12] Orbital point group symmetry should also be considered especially in the calculation of spectroscopic properties where selection rules are important; occasionally Rydberg orbitals might also be necessary.[13] All these considerations mean CAS/RASSCF is rather esoteric for the uninitiated, but we stress that orbital selection, which we do not flesh out here, is extremely important.[14, 15] Introductory guides can be found in chapter 4.6 of Ref 7 or chapter 14 of Ref 10.

Like HF, the multireference family is populated by a very large variety of dynamically correlated methods. Common examples include variations on multireference configuration interaction (MRCI) such as difference dedicated configuration interaction (DDCI),[16-21]

multireference Moller-Plesset (MRMPn) and restricted/complete active space perturbation theory (RAS/CASPTn),[22, 23] as well as multireference coupled cluster theory (MRCC) among others.[24-26] CASPT2, being the most affordable option, is of course most often encountered in the literature, although it should be noted that perturbation theory in general is susceptible to spurious issues, such as intruder states, which are not always foreseeable in the reference wavefunction.[27-30] Other methods have more limited application, but may be the only options capable of satisfactory outcomes for especially difficult problems.

RASSCF and many dynamical correlation methods are not size-consistent, i.e. the energy of a non-interacting dimer is the higher than the sum of each monomer considered in isolation. For large problems where this is a concern – typically more than 100 electrons – specialized methods such as second-order *N-Electron Valence State Perturbation Theory* (NEVPT2) and variations of MRCC ought to be considered.[31-33] This said, CASPT2 and MRCI are nearly size-consistent, and so are nonetheless popular options for investigations of multireference nitroxides of moderate size, such as the biradicals studied by Angeli et al.[32] and the many polyradicals modelled by Barone et al.[34-42]

6.2.3 Single-Reference Methods for Strongly Correlated Systems

For predicting ground state multiplicities and estimating useful properties such as singlet-triplet (S–T) energy gaps, one may appeal to one of several single reference methods which are considerably cheaper.[43] These tend to operate under a similar *modus operandi*, *i.e.* a strongly correlated low-spin state, such as an open-shell singlet, is estimated by projection or spin excitation from a much less correlated high-spin reference, typically a triplet, quintet *etc*. for which the single reference approximation is valid.

The simplest approach can be found in *broken-symmetry* density functional theory (BS-DFT),[44-47] a method which works within the *unrestricted* Kohn-Sham formalism (UDFT), where the spatial components of MOs are allowed to differ. Owing to its computational efficiency, UDFT is often a first approximation for modelling open-shell systems. However, unrestricted wavefunctions suffer from a serious issue known as the *spin contamination error*, the artificial mixing of higher spin states into the wavefunction in such a way that the total spin is greater than its formal value.[48] Strongly correlated problems tend to be highly spin-contaminated, so a direct UDFT calculation on for instance, an open-shell singlet, will certainly be erroneous.[49] The BS-DFT method resolves this issue via spin projection.[44-47] In the simplest case, a contaminated BS singlet is referenced to the negligibly contaminated triplet state which results in the following expression for the vertical S–T gap,[50]

$$\Delta_{S-T}^{vert} = \frac{2(E_{BS}-E_T)}{\langle S_T^2\rangle-\langle S_{BS}^2\rangle} \qquad (3)$$

such that the true singlet energy can be approximated as,

$$E_S = \Delta_{S-T}^{vert} + E_T \qquad (4)$$

where E_{BS} is the electronic energy of the contaminated BS singlet, E_T is the energy of the triplet, at the BS singlet geometry, and $\langle S_{BS}^2\rangle$ and $\langle S_T^2\rangle$ are the total spin eigenvalues of the BS singlet and triplet states respectively. Numerical values for these quantities are printed in the output of most quantum chemistry codes. The adiabatic S–T gap may be written as,

$$\Delta_{S-T}^{adia} = \frac{2\left(E_{BS^i} - E_{T^i}\right)}{\langle S_{T^i}^2\rangle - \langle S_{BS^i}^2\rangle} + E_{T^i} - E_{T^j} \quad (5)$$

or in its approximate form,

$$\Delta_{S-T}^{adia,approx} = \frac{2\left(E_{BS^i} - E_{T^j}\right)}{\langle S_{T^j}^2\rangle - \langle S_{BS^i}^2\rangle} \quad (6)$$

where i and j indicate the optimised geometries of the BS singlet and triplet states respectively. A suitable guess for the BS singlet can be accomplished by mixing the HOMO and LUMO orbitals of a closed-shell UDFT singlet (e.g., by invoking the `Guess=Mix` keyword in Gaussian) thus breaking the spin symmetry of the singlet wavefunction. This method is not limited to singlet-triplet couples and a generalisation can be made for any low-spin, high-spin dimer.[51-56] The quality of the projection is quite sensitive to one's level of theory. Global hybrid functionals such as B3LYP, BMK and M06-2X are recommended,[57, 58] although we tend to advise use of the latter for more reliable treatment of organic radicals. Adiabatic gaps are typically improved through the inclusion of zero-point corrections to the energy terms.

A more robust strategy for ground-state calculations is the spin-flip (SF) ansatz of Krylov *et al*.[59] These methods involve an excitation operator whose action is to perform a spin-flip type excitation of an electron from the reference wavefunction thus changing its multiplicity.[59] In simple terms, a set of low-spin configurations, constituting the strongly correlated problem, are spawned by flipping unpaired electrons in the frozen basis of MOs constituting a high-spin reference. The quality of the resultant wavefunction hinges on the quality of the reference, which in the single reference framework can be systematically improved forming a familiar hierarchy, *i.e.* SF-SCF/SF-DFT through to SF-MP2 and high-order SF-EOM-CC *etc.*[60-64] The SF operator is perfectly compatible with a UHF, although a *restricted open-shell* (ROHF) reference, where each electron pair is confined to a pair of degenerate MOs, has been shown to benefit predictive power.[65] Several "spin-correct" techniques, that attempt to rectify the spin-contamination problem, have been proposed in recent literature.[66-68]

Another popular addition to the single reference family is the RAS-SF approach of Casanova *et al*.[69] In this method, the active space is defined under the usual RAS specifications for a ROHF high-spin reference. A larger and more general set of determinants is subsequently generated, describing a wavefunction that is spin-complete and size-consistent.[70] One particular advantage of RAS partitioning is in its regular treatment of polyradicals of arbitrary degree, as these ordinarily pose something of a challenge to single reference methods. Like RASSCF however, active space specification has great influence on the quality of the wavefunction, not neglecting the exponential scaling in the number of determinants generated (although scaling with molecular size with a fixed active space is manageable). Recent implementations of RAS-SF also permit a degree of orbital relaxation, admitting this scheme to the multireference family of methods.

6.2.4 Selected Applications

Case Study 1: The role of the multiconfigurational character of nitronyl-nitroxide in the singlet–triplet energy gap of its diradicals.[41] This recent publication by the Barone group illustrates some of the caveats that must be considered when applying a multi-reference solution to a typical problem. In this case, the effect of the active space on the quality of

calculated *singlet-triplet* (S-T) energy gaps for three *nitronyl-nitroxide* (NN) based diradicals (Figure 6.1) were assessed for the multireference, dynamically correlated DDCI method and is simplified variant, DDCI2. ROHF/6-311G(d) calculations of the triplet states for each species were initially performed on their X-ray crystal structures in the software package GAMESS. For each diradical, an *Ad hoc* fragmentation was then undertaken, and the dimensionality of the problem for the multi-reference component was reduced to the most pertinent features (shown as blue in Figure 6.2), after which the active space was defined. DDCI calculations were then performed in the BALOO code, an inhouse program developed independently by Barone for these problems.

INSERT FIGURE 6.2

Several interesting observations can be made from this work. For reliable treatment of polyradicals involving an NN radical, it was speculated that the CAS reference must include at least three orbitals and electrons for satisfactory agreement with experiment, i.e. one for each N-O fragment and a third for the central carbon. Thus, S-T gaps for Ullmann's diradical (see Figure 6.2), was only accurately approximated (i.e. with transition frequencies between 90 - 110% of experimental values) with a CAS(6,6) reference involving the LUMO+2 to HOMO-3 MOs, as these encapsulate both features as well as the linker. The minimal CAS(2,2) reference involving only the magnetic HOMO and HOMO-1 orbitals was woefully inadequate in every example, resulting in transition frequencies of 10-30% of experiment. Unsurprisingly, DDCI2 was found to be less reliable than DDCI with the low-quality CAS(2,2) reference. However, the performance became comparable when the (6,6) active space was included. This highlights one of the many subtleties of multi-reference calculations, namely, the balance between a more complete (read larger) active space, and a more rigorous (read reliable) method for a given allocation of computational resources.

Case Study 2: Spin coupling interactions in C=C or B–B-cored porphyrin-mimetic graphene patch nitroxide diradicals.[71] A useful example of both single and multireference methodologies can be found in this recent article on the S-T energy gaps for an isomeric family of C=C, and B-B coupled porphyrin bridged nitroxide diradicals (Figure 6.3). These larger systems are practically out of reach for most multi-reference methods, but typical of the problems quantified with single-reference approximations in the literature. In this case, gas phase BS singlet and triplet structures were first optimized in Gaussian with UB3LYP/6-311G(d,p). BS-DFT predictions of the adiabatic S-T gap were then estimated using Yamaguchi's approximate expression, with subsequent calculations of the SF-DFT energies obtained from single point SF-PBE50/6-311G(d,p) and SF-5050/6-311G(d,p) calculations performed in Q-Chem.

INSERT FIGURE 6.3

The results of this comparison are useful, as they highlight the deficiencies one is likely to encounter when compromising with a single-reference method. Interestingly, both BS- and SF-DFT are in complete agreement as far predicting the ground-state multiplicities is concerned, (i.e. the sign of the S-T gap) however the disagreement in the energy itself is quite dramatic (with BS-B3LYP predicting ~30% of the SF-DFT average). The authors complete the remainder of their calculations with BS-B3LYP. However, it is very difficult to comment on which approach is most reliable given the absence of an experimental reference (which is often the case), or a high-level computational reference.

6.2.5 Concluding remarks

Correct application of multireference methodology is something of an acquired art. The approach used and its accuracy will vary depending of the nature of the problem and / or the resources available to handle it. CAS and RASSCF are available in most quantum chemistry software packages and are useful as a first approximation. However, neglect of the dynamical component will not lead quantitative agreement with experiment in most cases. For this methods such as MRCI or high-level perturbation theory, up to CASPT3, is required and for these we recommend the licensed packages MOLPRO or MOLCAS. As for MRCC, the powerful implementation of Kallay et al.[72] is promising but limited to a stand-alone package of the same name. Fortunately, the code is free for academic use and may be interfaced through the MOLPRO environment. These packages possess somewhat complex input formats that can be unfriendly to the less-experienced user. More agreeable platforms can be found in ORCA or DALTON, the latter of which is also open-source. Any package supporting DFT is suitable for BS calculations, although the SF methods are mostly limited to Q-Chem. In all cases, we advise readers to consult the relevant manual entries before setting any unfamiliar calculations.

6.3 Computation of Electron Paramagnetic Resonance Spectra

Given the range of applications in which nitroxide radicals are formed and take part in chemical reactions, monitoring the formation and presence of the nitroxide radical species can be desirable. To that end, electron paramagnetic resonance (EPR) spectroscopy is an extremely useful technique and a one that can be complemented with quantum chemistry simulation to help assign complex spectra and relate that to the underlying structural properties of the radical. Fundamentally, EPR involves measuring the energy at which the magnetic moment of an unpaired electron is flipped in the presence of an external magnetic field (Figure 6.4). To simulate the resulting spectra, one first needs parameters (the g-factor and hyperfine splitting constants, defined below) describing the response of the electron to the magnetic field, and one then needs to take into account the experimental environment and aspects as the tumbling regime and whether the magnetic field is continuous or pulsed. Quantum chemistry can help with the former, and the methodology developed for this purpose is outlined below (section 6.3.1), while the methodology for the latter is briefly outlined in section 6.3.2.

INSERT FIGURE 6.4

6.3.1 Computing *g*-Tensors and Hyperfine Coupling Constants with Quantum Chemistry.

The main working equation of EPR is given by:

$$\Delta E = h\nu = g_e \mu_B B_0 \qquad (7)$$

where: g_e is the electronic *g*-factor (approximately 2.0 for a free electron), μ_B is the Bohr magneton, and B_0 is the external magnetic field strength. Electrons are not, however, “free” in a molecule, as they will interact with both the external magnetic field and internal magnetic fields generated by the nuclei. This generates an effective magnetic field, B_{eff}:

$$B_{eff} = B_0(1 - \sigma) \qquad (8)$$

where σ includes local magnetic effects. Eq. (8) can then be rewritten as:

$$h\nu = g\mu_B B_0 \qquad (9)$$

where:

$$g = g_e(1 - \sigma) \qquad (10)$$

Here, *g* is referred to as the *g*-factor. A value of *g* that is significantly different to the constant g_e term can give information about the molecular orbital in which the unpaired electron resides. In reality the *g*-factor is a second-rank tensor, selection of an appropriate coordinate system, for example Cartesian coordinates, allows the 3x3 matrix to be diagonalized to give g_{xx}, g_{yy}, and g_{zz}. Another consequence of the interaction between an unpaired electron and atomic nuclei is hyperfine splitting, which arises due to coupling between electronic and nuclear spins. This reveals itself in spectra as multiple peaks, centred at $h\nu$, and the so-called "multiplicity" of a transition can be complex.

Spectroscopic methods study the response of a system with respect to some external perturbation, and the energy can therefore be expanded as a Taylor series:

$$E(X) = E(0) + \left.\frac{\partial E}{\partial X}\right|_{X=0} \cdot X + \frac{1}{2!}\left.\frac{\partial^2 E}{\partial X^2}\right|_{X=0} \cdot X^2 + \frac{1}{3!}\left.\frac{\partial^3 E}{\partial X^3}\right|_{X=0} \cdot X^3 \ldots \qquad (11)$$

where X is an external perturbation. The calculation of g-factors is no different in this respect, in that it is the second derivative of the many-electron energy with respect to an external magnetic field and the overall net spin component in a given direction (Eq. 12).

$$g_{xx} = \frac{1}{\mu_B}\left.\frac{\partial^2 E}{\partial B_x S_x}\right|_{S=B=0} \qquad (12)$$

As a result of this well-defined expansion, computation of EPR *g*-tensors is generally possible by both analytical and numerical methods in most electronic structure packages for a range of quantum chemistry methods, generally HF, DFT, and MP2. Traditionally, magnetic property calculations have suffered from gauge invariance; when using an approximate wavefunction the results of the calculation change depending on the orientation of the molecule in the Cartesian frame of reference. This is negated by using, for example, Gauge-Invariant Atom Orbitals (GIAO) which ensure exact gauge invariance, or by using a large enough basis set that the invariance becomes negligible. In reality, unless the choice of gauge origin is very poor, the effects of gauge invariance are not large enough to render a calculation useless, however most modern electronic structure packages offer formally invariant methods and their usage is recommended.

The second property of interest are hyperfine splitting constants, arising from the different possible nuclear and electronic spin configurations. For these properties, several terms need to be computed:

1. The isotropic Fermi contact term, which describes the magnetic interaction between an electron and a nucleus, is required and calculated from:

$$a_{iso}(N) = \left(\frac{4\pi}{3}\langle S_z\rangle^{-1}\right) g_e g_N \beta_e \beta_N \rho(N) \qquad (13)$$

where $\langle S_z \rangle$ is the expectation value of the z-component of the total spin, g_e and g_N are the electron and nuclear g-factors, respectively, and β_e and β_N are the electron and nuclear magnetons, respectively. The Fermi contact integral, $\rho(X)$, can be computed as:

$$\rho(N) = \sum_{\mu\nu} P_{\mu\nu}^{\alpha-\beta} \varphi_\mu(r_N)\varphi_\nu(r_N) \qquad (14)$$

where $P_{\mu\nu}^{\alpha-\beta}$ is the one-electron spin-density-difference matrix, computed as the difference between the spin density matrices of the α and β electrons), and evaluation of the overlap of the φ_μ and φ_ν basis functions is at nuclear position r_x. For brevity, P_N is commonly used in place of $g_e g_N \beta_e \beta_N$.

2. The spin dipole component, computed as the expectation value over the spin density:

$$A_{kl}^{dip}(N) = P_N \sum_{\mu,\nu} P_{\mu\nu}^{\alpha-\beta} \langle \varphi_\mu \left| r_N^{-5} \left(3\vec{r}_k \vec{r}_{N_l} - \delta_{kl} r_N^2\right) \right| \varphi_\nu \rangle \qquad (15)$$

where $\vec{r}_N$ is a vector that points from the nucleus of interest to an electron.

3. The second-order spin-orbit coupling term:

$$A_{\mu\nu}^{orb}(N) = -\frac{1}{2S} P_N \sum_{\mu\nu} \frac{\partial P_{\mu\nu}^{\alpha-\beta}}{\partial B_k} \langle \varphi_\mu \left| h_l^{SOC} \right| \varphi_\nu \rangle \qquad (16)$$

Two key points about Eq. 13 and 14 are the computed isotropic contact term is dependent on the quality of the spin-density matrices of α and β electrons, and on the overlap between basis functions at nuclear positions. The quality of the spin-density matrices is generally affected most by the method used to compute them. As all systems with unpaired spins are open shell, restricted MO theory, for example restricted Hartree-Fock (RHF), is not applicable. Its restricted open-shell counterpart, ROHF, is also found to generally perform poorly as only the singly occupied molecular orbital (SOMO) will contribute to $P_{\mu\nu}^{\alpha-\beta}$, as the spatially identical doubly occupied orbitals will have zero spin-density difference. This can result in the incorrect prediction of zero hyperfine coupling for atoms in the nodal plane of the SOMO. Unrestricted HF (UHF), on the other hand, optimizes both α and β orbitals, and can account for spin polarization. Unfortunately, UHF wavefunctions often suffer from spin contamination, arising from the mixing of higher spin states into the wavefunction, and this too will result in less accurate spin-density matrices. Projected UHF methods can be used to project out spin contamination to improve results.

Alternatively, one may turn instead to methods that suffer less from spin contamination; indeed, most electronic structure packages offer hyperfine coupling constant calculations with some of the most powerful electronic structure theories, for example coupled cluster (CC) methods, as well as with DFT. If CC methods are too expensive, DFT methods are generally robust however, as always, it is recommended the functional of choice is benchmarked for suitability before predictions are made.

The second issue is that of appropriate basis set selection. As the basis set overlap is computed at nuclear positions, those with the largest contributions to the splitting constants describe the core s orbitals. However, the most popular basis sets, for example those of Pople or Dunning, do not describe the core region with the same flexibility as the valence region. This is due to their emphasis on accurate calculations of bonding phenomena, to which core electrons contribute little. As well as this, atomic s orbitals exhibit an electron cusp at the

nucleus, which is not well captured by Gaussian-type orbitals (GTO). To that end, basis sets have been developed that systematically improve the description of the core region of electrons, examples being EPR-II or EPR-III, and their usage is recommended. A second practical consideration when using DFT is to ensure that a large numerical grid is employed, to ensure numerical integration remains accurate.

Although not necessarily common when exploring the chemistry of nitroxide radicals, it is possible one may encounter heavy elements, and under these circumstances relativistic effects may become significant. Unlike if bonding interactions are being studied, in which case the relativistic core electrons can be replaced by an effective core potential (ECP) which may include relativistic effects in its parameterisation, accurate EPR calculations generally require the explicit treatment of electrons. As a result, all-electron approximations are available in most electronic packages, and their use is recommended.

6.3.2 Simulating EPR Spectra

The computational simulation of EPR spectra depends not only the magnetic properties of the molecule (splitting parameters, spin active nuclei present, linewidth and g tensor values) but also the experimental conditions, such as the type of tumbling regime and whether the spectrum is collected as a continuous-wave (cw) EPR spectrum or under pulsed conditions. Many programs have been developed simulate spectra, including Easyspin,[73] Winsim,[74] XSophe,[75] and MoSophe.[76] More specialist programs such as WinMOMD[77] for simulation of slow-motional spectra using the MOMD (microscopic order, macroscopic disorder) model, and optimised SLE solvers employed by Freed[78] at the ACERT Center at Cornell have been employed for more targeted systems. Generally speaking, these programs make use of inputted parameters (splitting parameters, spin active nuclei present, linewidth and g tensor values) in order to construct a parameterised spin Hamiltonian. These can be extracted from the experimental spectrum or, if one is trying to make a first principles prediction, these are provided from the quantum-chemical studies described above. A quantum-mechanical approach is then used to simulate the resulting spectrum according to the type of tumbling regime (i.e., isotropic limit, fast motion, slow motion, or rigid limit) and whether the spectrum is collected as a continuous-wave (cw) EPR spectrum or under pulsed conditions. Details of how EPR spectra are simulated are covered in Chapter 4.

6.3.3 Selected Applications

Case Study 1: DFT Calculations of Isotropic Hyperfine Coupling Constants of Nitrogen Aromatic Radicals: The Challenge of Nitroxide Radicals.[79] In this study, Hermosilla *et al.*[79] assess the performance of DFT for accurately predicting hyperfine coupling constants, using the PBE0 and B3LYP functionals in conjunction with several basis sets; 6-31G(d), N07D, TZVP, and EPR-III. The study utilised a test set of 38 nitrogen-containing radical species, with 15 of the species nitroxide radicals (Figure 6.5). As a result of the different coupling environments a total of 165 hyperfine splitting constants for ^{14}N and ^{1}H nuclei were calculated and compared with experimental data. The study highlights the importance of basis sets when calculating EPR properties, as well as the importance of comparing and contrasting DFT

results against HF or more advanced wavefunction methods, as the B3LYP results counter-intuitively suggest that 6-31G(d), rather than the larger, EPR specific EPR-III basis set, was more capable of accurately predicting EPR spectra.

INSERT FIGURE 6.5

Case Study 2. The temperature dependence of nitroxide spin–label interaction parameters: a high-field EPR study of intramolecular motional contributions.[80] This study used a combination of high-field W-band EPR and density functional theory calculations to study and explain the temperature dependence of the *g (anisotropic)*, a (hyperfine), q (quadrupole) tensors of two nitroxides, 3-hydroxymethyl-2,2,5,5-tetramethylpyrrolin-1-oxyl and 4-hydroxy-2,2,6,6-tetramethylpiperidine-N-oxyl, in glass-forming *ortho*-terphenyl solution. The experimental temperature dependencies were attributed to both the averaging of the anisotropies of the EPR parameters in the glassy matrix, and the intramolecular out-of-plane motion of oxygen in the nitroxide group. This latter mechanism was confirmed via DFT calculations whereby the B1LYP/SVP level of theory was first used to compute the structures associated with harmonic oxygen out-of-plane vibrations, and then the various tensors were calculated at each structure to show how the vibrational motion affected them (Figure 6.6). For this purpose, the SVP basis set was replaced with IGLO-III for computation of the a- and q-tensors; while for the g-tensor LSD/SVP was used in conjunction with RI-SOMF(1X) for the treatment of the spin-orbit coupling operator. Studies such as this highlight the important role of first principles theory in assigning or interpreting complex EPR spectra.

INSERT FIGURE 6.6

6.4 Predicting Oxidation Potentials

As redox active molecules possessing unique properties and reactivity, nitroxides are utilised in many applications ranging from energy storage devices[81-85] and oxidation catalysts[86-90] to redox mediators for solar-cells[91-94] and super-oxide dismutase mimics.[95, 96] Nitroxides can typically undergo an electrochemically reversible 1-electron oxidation to afford the corresponding oxoammonium cation (see Figure 6.7). In contrast, nitroxide reduction is usually electrochemically irreversible; spontaneous proton transfer from protic impurities rapidly quenching the initially formed oxyamine anion as a hydroxylamine. In this latter case, the highly coupled nature of the rate and equilibrium constants for the underlying elementary processes can make the direct experimental measurement of a corresponding potential difficult, and computational chemistry offers a valuable alternative to experiment.

INSERT FIGURE 6.7

Even when measurement is possible, the accompanying synthesis can be expensive and time-consuming, and as such computational chemistry offers an attractive means of assessing the utility of a given species prior to experiment. In this respect, the success or failure of a given nitroxide hinges on its precise redox properties; including the electrochemical reversibility of oxidation/reduction and the respective potentials of these electron transfers. For instance, in alcohol oxidation, nitroxides are frequently employed as catalysts in conjunction with a bulk stoichiometric oxidant, such as sodium hypochlorite or ambient oxygen (see Figure 6.8).[97, 98] This bulk oxidant, [O], is used to generate the catalytically active oxoammonium species *in*

situ, which in turn oxidises the substrate alcohol to a ketone. If the oxidation potential of the nitroxide is too high, then the bulk oxidant will be unable to oxidise the initial nitroxide into the catalytically active oxoammonium cation. Conversely, if the oxidation potential of the nitroxide is too low, then the oxoammonium cation will be unreactive towards the alcohol substrate. Moreover, in biochemistry nitroxides are of interest as antioxidants; protecting cells against cytotoxic reactive oxygen species.[99, 100] *In vivo*, both oxidation and reduction processes involving nitroxides are relevant,[101, 102] and so the ability to predict and rationalise the redox potentials of nitroxides is invaluable for screening novel antioxidants.

INSERT FIGURE 6.8

While other references discuss the theoretical evaluation of redox potentials for organic[103, 104] and inorganic[105] species in some detail, we will more briefly outline some of these considerations within the specific context of nitroxide oxidation and reduction. The theoretical calculations of most thermochemical quantities, including oxidation and reduction potentials, usually take advantage of the Born-Oppenheimer approximation, which partitions the electronic and nuclear wavefunction and so separates the calculation into three steps (Figure 6.9). Initially, the electronic energy of the molecule in its oxidised and reduced form is calculated using normal electronic structure calculations. Next, the entropic contribution from nuclear motion is calculated, usually employing harmonic or quasi-harmonic approximation in conjunction with computed frequencies. Finally, statistical averaging of relevant conformations and solvent corrections are applied, usually by assuming Boltzmann distributions and applying continuum solvent models. For computation of redox potentials, the first step affords the gas phase 0 K adiabatic ionization energy (IE) or electron affinity (EA), the second step computes the (temperature dependent) entropic corrections, while the third step corrects the resulting gas-phase free energy for solvent effects and appropriately weights these quantities according to the population of the individual conformations.

INSERT FIGURE 6.9

The main methodological challenges relate to the first and third steps: in the former case, obtaining a sufficiently accurate description of the electronic energies, albeit within a single reference framework; in the latter, modelling the effects of solvation, particularly for the ionic species. In addition, there is the added complication of converting the solution-phase Gibbs free energies for the half reactions into electrode potentials, which entails choosing appropriate values for the reference electrode, treating the electron in a consistent manner, and considering coupled chemical processes where relevant. Below we introduce the methods (and where relevant equations) for the each of these steps, before examining some of the applications.

6.4.1 Definitions and Key Equations

The standard reduction potential directly measures the thermodynamic feasibility of the general reduction half-reaction.

$$O\,(s) + n_e e^-\,(g) \leftrightarrow R\,(s) \qquad (17)$$

where *O* refers to an oxidized reagent, *R* refers to a reduced reagent, n_e is the number of electrons exchanged between the oxidized and reduced species, and "s" and "g" refer to

species in solution and in the gas phase, respectively. Note that the charge of O and R are not shown here but must be balanced across the reaction. The absolute reduction potential for this reaction is given by the Nernst equation[106, 107] as

$$\Delta_r G^o(O|R) = -n_e F E^o_{abs}(O|R) \qquad (18)$$

where: $\Delta_r G^o(O|R)$ is the Gibbs free energy change for the half reaction, F is the Faraday constant (96485 C mol^{-1}), and n_e is the number of electrons transferred in the half-reaction. To facilitate comparison with experiment, this must be converted to a relative (cell) potential measured against a reference electrode (such Fc/Fc+, Ag/Ag+, the standard hydrogen electrode, etc).

$$E^o_{rel,REF}(O|R) = E^o_{abs}(O|R) - E^o_{abs}(REF) \quad (19)$$

Here $E^o_{abs}(REF)$ is the absolute reduction potential of the reference electrode and in principle can be calculated the same way, though in practice literature values are available for most references.[103, 104] In choosing a literature value it is important to ensure that the treatment of the electron is consistent in both half reactions so that it cancels from the cell potential. While the electron has no electronic energy as such, it is assumed to have thermal energy and entropy, but the amount differs according to which convention is used. Details of the different conventions are in Refs 103, 104; ultimately, the choice of convention has no impact on the results provided it is applied consistently.

The values of $E^o_{rel,REF}(O|R)$ yielded from the above equations correspond directly to the experimental half-wave potential for reversible redox processes. However, many species (including nitroxides) can undergo irreversible redox reactions which are often coupled with other spontaneous proton transfer or addition/fragmentation processes. In these situations, experimental cyclic voltammograms (CVs) are complex. One can either fit these experimental CVs with kinetic schemes that take into account the redox processes, the coupled chemical reactions, and diffusion into and out of the double layer. In such cases the computational $E^o_{rel,REF}(O|R)$ can be compared with the fitted potentials obtained for isolated redox processes. Alternatively, one can use computational chemistry to study the coupled processes as well and yield adjusted half-wave potentials. For instance, in aqueous environments reduction of nitroxide radicals are accompanied by rapid protonation (Figure 6.10). As such, formal reduction processes can be represented by different half reactions, which will depend heavily the nitroxide of interest and on the pH of the solution. Thus, the 1-electron reduction of TEMPO$^\bullet$ generates a TEMPO$^-$ oxyamine anion, which is rapidly quenched by water (across a range of pH values) to form the corresponding TEMPOH hydroxylamine. However, the TEMPOH hydroxylamine is itself a weak base (conjugate acid pK_a = 6.9 – 7.5) and may be protonated depending on the pH of the solution. As a result, the half-wave reduction potential observed by experimental measurements is given by:

$$E_{1/2} = E_{red}(X^\bullet, 2H^+/H_2X^+) + \frac{RT}{F}\ln(K_1K_2 + K_1[H^+] + [H^+]^2) \qquad (20)$$

where $E_{red}(X^\bullet, 2H^+/H_2X^+)$, K_1 and K_2 are as defined in Figure 6.9.

INSERT FIGURE 6.10

6.4.2 Electronic Structure Methods and Gas-Phase IEs and EAs

Electronic structure methods are conveniently divided into two categories; wavefunction-based approaches and density functional theory (DFT). Within wavefunction theory there are

a hierarchy of different approximations with varying levels of accuracy, some of which were briefly introduced in section 6.2. For redox potentials, single reference methods are usually sufficient. There are three main 'families' of correlated single-reference wavefunction methodologies: Møller–Plesset perturbation (MP*n*) theory[108-114] (e.g. second-order Møller–Plesset corrections, MP2), couple cluster (CC) theory[115-117] (e.g. single, double and perturbative triple excitations, CCSD(T)) and finally configurational interaction (CI) theory[117-119] (e.g. quadratic configurational interaction with single, double and perturbative triple excitations, QCISD(T)). While acceptable accuracy will depend largely on context, a sufficiently accurate treatment of electron correlation is achieved in most chemical systems with CCSD(T) or QCISD(T) used in conjunction with large triple zeta basis sets. Such energies will (usually) only differ from corresponding exact values by 1-2 kJ mol^{-1}.[120, 121] Thus, CCSD(T) is frequently labelled the "gold-standard" of computational chemistry, as this level accuracy is sufficiently accurate for most (single-reference) applications.

Composite procedures are a notable subclass of wavefunction-based approaches that pragmatically perform basis set extrapolations schemes and/or combine the results of calculations performed at different levels of theory. These procedures are usually as accurate as the large basis set CCSD(T) (or equivalent) calculations that they are attempting to approximate, but only require a fraction of the computational expense.[122-126] The Gaussian *composite procedures*[122-126] (G*n*), originally developed by Curtiss and co-workers are among the most popular, and a popular variant of G3 theory is the less computationally intensive G3(MP2)-RAD procedure.[127] Other well-known *composite procedures* include the CBS methods[128-135] developed by Petersson and co-workers, and the W*n* methods[121, 136-138] formulated by Martin and co-workers. Although not strictly a composite procedure, the F12 approximation[139] in its various manifestations also delivers improved accuracy by significantly reducing errors caused by small basis sets.

Density functional theory (DFT) calculates the energy of a molecule or atomic species using its one-electron density and a functional. The Hohenberg-Kohn Theorems,[140] which form part of the inspiration for DFT, state:

> 1) That the ground state external potential (and thus total electronic energy of the ground state) is a unique functional of the electron density.
>
> 2) That a density that minimizes the total energy of the ground-state is the exact ground-state density.

Using the electron density to obtain the total energy has been touted as a way of circumventing the poor size scaling of wavefunction based methods. Unfortunately, the first Hohenberg-Kohn Theorem is not constructive but rather an existence proof. As such, it only establishes that the ground state external potential is a unique functional of the electron density and provides no insights into its actual mathematical form. Consequently, the exact DFT functional is unknown.

Modern DFT functionals are based on the Kohn-Sham equations,[141] which cleverly consider the Hamiltonian for a fictitious system of *non-interacting electrons* that have an overall ground-state density that is identical to the real atomic or molecular system (where the electrons are allowes interact). Ideally, DFT would be exact and formulated from fundamental physical and mathematical arguments. However, in practice many popular DFT functionals are heavily parametrized using test sets of experimental and (wave-function derived) theoretical data. While current DFT functionals offer reasonable accuracy at low

computational cost, they can also fail spectacularly and unexpectedly.[142] Many of the most popular functionals, such as B3LYP, have been found to fail dramatically (often to the extent that results are qualitatively incorrect).[142] Moreover, there is no systematic way to improve DFT results and so choice of functional is quite subjective. Because of this often variable and unpredictable accuracy, DFT should always be employed cautiously in conjunction with appropriate benchmarking.

There are many articles that evaluate the performance of common DFT functions and other wavefunction-based methodology for the calculation of IEs and EAs. For instance, our group examined theoretical procedures for IE and EA calculations on a range of piperidine, pyrrolidine, oxazolidine derivatives, isoindoline, and azaphenalene nitroxides.[143] This study revealed that low cost DFT procedures often carried unacceptably large errors, with B3LYP and MPWB1K carrying mean absolute deviations (MAD) for EAs of 0.23 and 0.40 eV, respectively. Interestingly, these errors are primarily associated with the reaction site and can be largely mitigated using an ONIOM partitioning scheme. For instance B3LYP in conjunction with a G3(MP2)RAD core affords much smaller deviations (around 0.10 eV). Pantazis and co-workers recently examined the IEs of 19 organic species with several methods using CCSD(T)/CBS data as a reference (see Figure 6.11).[144] Despite its enormous popularity in computational organic chemistry, B3LYP once again performs relatively poorly with mean absolute deviations and maximum deviations (MAX) of around 0.40 and 0.70 eV, respectively. M06-2X performs better with a MAD of only 0.11 eV, although it still suffers an unexpectedly large MAX (for phenol) of nearly 1 eV. CCSD(T)/cc-pVTZ offers excellent accuracy, with MAD and MAX values of 0.14 and 0.16 eV, respectively. However, this accuracy is strongly basis set dependent. If a smaller double-zeta basis set (cc-pVDZ) is employed, the MAD and MAX of CCSD(T) increase dramatically to over 0.4 V. CCSD(T)-F12 offers an excellent compromise, with a double-zeta F12 calculation essentially matching the accuracy of standard triple-zeta CCSD(T).

INSERT FIGURE 6.11

6.4.3 Solvent Effects and Redox Potentials

To convert gas-phase IEs and EAs to redox potentials, one needs to calculate the Gibbs free energies of solvation, so as to obtain Gibbs free energies in solution. In doing this one also needs to include a term $RT(\ln V)$ to account for the change of state from 1atm to 1M.[145] The simplest and most computationally efficient methods for calculating solvation Gibbs free energies are continuum models, in which each solute molecule is embedded in a cavity surrounded by a dielectric continuum of permittivity ε.[146] Continuum models are designed to reproduce bulk or macroscopic behaviour, and can fare extremely well in certain applications including redox potentials.[147] However, the results obtained using continuum models are highly sensitive to the choice of cavities (which are typically parameterised to reproduce the free energies of solvation for a set of small organic molecules). This reliance on empirical parameterisation means the errors can sometimes be unpredictable. Moreover, their accuracy can suffer if there are explicit solute-solvent interactions such as complex formation or hydrogen bonding.[148] Although this problem can be overcome by including a small number of explicit solvent molecules in the ab initio calculation, as in a cluster-continuum model,[149] this adds significantly to the cost of the calculation.

As a result, in small to medium nitroxides (where high-level composite calculations are feasible), the accuracy of redox calculations is usually limited by the accuracy of the continuum solvent model. This is particularly a problem because of the involvement of charged species. For neutral molecules, solvation energies are typically small, and many solvent models are able compute the solvation energies of neutral molecules with reasonably high accuracy, with errors typically of the order of 5-10 kJ/mol.[150] However, errors in solvation energies for charged systems can be significantly larger (often above 20 kJ/mol; see Figure 6.12). This introduces correspondingly large errors into the resulting redox potentials. Fortunately, errors introduced by solvation models are often highly systematic (see Figure 6.13); depending on the functionality of anion or cation in question. Note that in Figure 6.13, the superior absolute performance of PCM-UAKS B3LYP is not a general result for other redox systems, and in other studies of nitroxides and or closely related species methods such as SMD or COSMO-RS perform better.[151-156]

INSERT FIGURE 6.12

INSERT FIGURE 6.13

Nonetheless, for the most part, errors in solvation energies within a set of related molecules are relatively systematic. As a result, they can be circumvented somewhat by computing redox potentials in an isodesmic fashion, where relative (rather than absolute) potentials are computed against a structurally similar reference system. The potential of the substrate is then determined by using this relative potential in conjunction with an accurate experimental value for the reference couple (see Figure 6.14). This approach exploits systematic error cancelation by offsetting the errors introduced by sub-optimal solvation modelling of both charged species. While this approach normally delivers more accurate potentials, it relies on the availability of accurate experimental measurements for the reference couple.

INSERT FIGURE 6.14

6.4.4 Selected Applications

Computational chemisty offers not only the opportunity predict kinetics and thermodynamics; it can also be used to help interpret the underlying structure-reactivity trends by providing detailed structural information, dipole and quadrupole moments, and other related properties. This in turn is useful in reagent design, as these case studies below illustrate.

Case Study 1. Computational Design of Cyclic Nitroxides as Efficient Redox Mediators for Dye-Sensitized Solar Cells.[157] With decreasing global fossil fuels reserves and increasing energy demand, improving the efficiency and cost-effectiveness of renewable energy is becoming an increasing priority. Dye-sensitised solar cells (DSSCs) are particularly promising, as they are less expensive and more flexible than traditional Silicon-based cells. DSSCs are a photoelectrochemical system consisting of two separate electrodes; a mesoporous thin-film semiconductor (usually TiO_2) with a tethered monolayer of sensitizing dye and a counter electrode (see Figure 6.15). An electrolyte containing a redox mediator is injected between these two electrodes. Light is first absorbed by a dye, then the photoexcited dye (S*) transfers an electron to TiO_2. The oxidised dye ($S^{+\bullet}$) is reduced by the redox mediator ($Md^{\bullet}$), with the oxidized mediator (Md^{+}) diffusing to the counter-electrode. There the oxidised mediator is

reduced by current passing through the cell. As it affects the electrochemical potential at the counter electrode and semiconductor, the redox mediator is a crucial component of the cell.

INSERT FIGURE 6.15

Nitroxides are particularly attractive as redox mediators because of their rapid and (usually) reversible redox chemistry, low toxicity, and low corrosivity. They are also characterized by fast rates of both heterogeneous electron-transfer and electron self-exchange reactions. Importantly, their oxidation potentials are also reasonably close to the optimal range of 0.60–0.85 V (versus SHE) and can be further optimised through structural modifications. However, this reversibility is fundamentally dependent on their chemical structure; with some cyclic nitroxides undergoing irreversible ring opening processes or fragmentation (Figure 6.16). Experimental cyclic voltammetry measurements can readily establish the oxidation potential of a given nitroxide and its electrochemical reversibility. Synthesis and characterisation of nitroxides is often time-consuming and expensive. Hence, computational screening is a particularly attractive; allowing for rapid and accurate prediction of the redox properties of candidate nitroxides.

INSERT FIGURE 6.16

To address this problem, we studied the nitroxide structural features to help guide experimental optimisation of DSSCs.[157] As redox mediators for DSSCs, nitroxides need to have oxidation potentials of 0.60 –0.85 V (vs SHE) and high stability. It was found that most monocyclic nitroxides had potentials in the correct range, but were susceptible to the ring-opening processes of Figure 6.16. These ring opening processes could be largely supressed by fusing aromatic rings to piperidine and pyrrolidine nitroxides, leading to azaphenalene and isoindoline ring frameworks. These basic frameworks are resistant to oxidative ring opening, as the initially formed nitroso and carbocation are held near each other by the secondary aromatic scaffold (and rapidly couple). However, their oxidation potentials that are too high for DDSCs (1.02 V and 0.98 V, respectively). One possible solution is replacement of the flanking groups with higher alkyls. While calculations indicate this substitution does appreciably lower the oxidation potential of isoindolines, unfortunately it also facilitates a β−fragmentation process that decomposes the oxoammonium species into a nitronone (Figure 6.16). Aside from modification of the flanking alkyl groups, introduction of electron donating amino subsitutents onto the aromatic ring also lowered the potential of isoindoline and azaphenalene based nitroxides. However, this moiety can also undergo irreversible oxidation with proton loss to form electrochemically inert products. As such, isomers bearing the NH_2 group are unsuitable for the present study.

However, it was shown that there are still nitroxides that possess oxidation potentials within the target range and meet the reversibly criteria outlined above. These included an adamantine-like species, piperidines with α-cyclohexyl groups, TMAO derivatives with alkyl and methoxy substituents, as well a large fused antiaromatic system (Figure 6.17). Latter experimental testing by Nishide and co-workers verified that one of these, the 2-azaadamantan-N-oxyl radical was an exceptional redox mediator, consistent with our theoretical predictions.[158] Employing this mediator in a DSSC, Nishide and co-workers set the benchmark efficiency (for organic radical based mediators) of 8.6%; significantly improving on the previous efficiency of TEMPO-based DSSCs of 5.4%.

INSERT FIGURE 6.17

Case Study 2. Effect of heteroatom and functionality substitution on the oxidation potential of cyclic nitroxide radicals: role of electrostatics in electrochemistry.[159] Computing accurate oxidation potentials is undoubtably helpful, as it enables the pre-screening of novel nitroxides for specific applications. However, using theory to deduce quantitative (or semi-quantitative) structure-reactivity or structure-property relationships is arguably even more useful because it allows nitroxides to be rationally designed for a specific purpose. Many theoretical and experimental studies rationalise nitroxide oxidation and reduction potentials using strain-arguments based on ring-size and rigidity.[98, 143, 157, 160, 161] Normally, the basis for such arguments is that the oxoammonium cation, oxyamine anion and nitroxide radical prefer different degrees of planarity around the nitrogen atom. Thus, attaining the optimal geometric rearrangement is hindered to varying extents by size and rigidity of the primary nitroxide ring. To examine strain-based arguments in more detail, we collated literature[143,157] high-level theoretical predictions of the oxidation and reduction potentials of prototypical nitroxides; separately examining the influence of ring contraction and rigidification.

INSERT TABLE 1

As Table 1 reveals, reduction potentials are significantly lowered by ring-contraction, with a decrease of around 140-180 mV. This indicates the larger piperidine (and azaphenalene) rings are better able to accommodate the geometric changes associated with nitroxide reduction as compared to the smaller pyrrolidine (and isoindoline) rings; consistent with a strain-based argument. Surprisingly, however, ring-size alone does not appreciably influence oxidation potentials; with minimal change moving from piperidine to pyrrolidine (or moving from azaphenalene to isoindoline). While aromatic rigidification does significantly increase oxidation potentials (by 240–260 mV), inexplicably, it also raises the respective reduction potentials (by 120-150 mV). In other words, oxidation potentials are insensitive to ring-size but increase substantially upon rigidification, while reductions potentials are lowered by ring-contraction yet raised by rigidification. Interestingly, rigidification of piperidine through the inclusion of multiple aliphatic frameworks lowers the respective oxidation potential (see Figure 6.17); indicating different effects from aromatic and aliphatic rigidification strategies. Collectively, this behaviour is incompatible with a simple strain-based argument. If attaining the optimal cation or anion geometry is hindered by ring size and rigidity, then why do these parameters appear to operate independently and have unpredictable effects on oxidation and reduction behaviour? Why does rigidification with aromatic (but not aliphatic) frameworks increase nitroxide oxidation potentials?

To address these questions, we recently explored if the fundamental electrostatics could rationalise nitroxide oxidation (and reduction) potentials.[159] Electrostatic effects can be described using a multipole expansion, which includes contributions from monopole, dipole, quadrupole and octapole (etc) terms. For electronically uncharged substituents, the dipole term is the first non-zero contributor to this expansion and so formed the basis for our initial investigations. The substituent orientation relative to the >N–O$^{\cdot}$ moiety is crucial, as this axis defines the only component of the dipole moment that will have a non-zero interaction with the charge formed upon oxidation. To decouple the dipole moment of the substituent from that of the >N–O$^{\cdot}$ group, we used analogues in which the >N–O$^{\cdot}$ moiety was replaced with a CH_2 group. This substitution conveniently preserves the relatively fixed orientations of the interacting substituents, as the basic C–C framework of these models is analogous to that of the corresponding nitroxides. Initial investigations revealed that this distance scaled dipole moment was very well correlated with experimental oxidation potentials. However, 3

nitroxides from this initial set possessing π-functionality were found to be significant outliers. This led us to investigate if this behaviour, and more generally the effect of aromatic rigidification on redox potentials (as reported in Table 1), could be electrostatic in origin.

The importance of quadrupole moments in the electrostatic description of molecules with π systems is well known.[162-164] Moreover, truncating the multipole expansion at the dipole term is only valid if the substituent and >N^+=O moiety are sufficiently separated, so at short-range higher order multipole terms may be significant. Inclusion of an appropriately scaled quadrupole term corrects the 3 previous outliers and simultaneously improves the correlation with the experimental oxidation potential. Moreover, this dipole-quadrupole parameter can be applied successfully to a total test set of 35 different α-tetramethyl substituted nitroxides; comprising of 1 pyrrolidine, 2 pyrrolines, 11 isoindolines, 15 piperidines, 2 morpholines, 3 azaphenalene and 1 azepine (Figure 6.18).[159] Despite the structural diversity of these nitroxides (including different ring sizes and rigidity), good correlation was observed between the distance scaled dipole and quadrupole term and the respective oxidation potential (total R^2 = 0.84). Reassuringly, the optimal ratio between the component dipole and quadrupole terms found via a 2-variable regression (1.78:1) is reasonably similar the theoretical ratio predicted in a multipole expansion (2:1). We should caution that due to relatively small separation between the nitroxide moiety and the substituent, higher order multipole moments may also contribute; particularly in more electrostatically complex systems. It is also important to note that this analysis only considers the underlying (gas-phase) electrostatic effects and does not account for other key factors including; induction, ring-strain, through space orbital overlap and solvent effects. Notwithstanding these considerations, this study highlights how nitroxide oxidation potentials can be rationalised with chemical intuition using substituent-based electrostatic arguments.

INSERT FIGURE 6.18

Returning briefly to the trends reported in Table 1, we can now fully rationalise these redox potentials in terms of strain and electrostatics. Strain-based effects are clearly a factor in the case of nitroxide reduction (where geometry relaxation is normally more significant). However, rigidification through the inclusion of fused aromatic rings introduces a large quadrupole moment. In the case of isoindolines and azaphenalenes, this quadrupole interacts unfavourably with the forming oxoammonium cation thereby raising the oxidation potential of the corresponding nitroxide. Conversely, this quadrupole interacts favourably with the oxyamine anion and so also raises the corresponding nitroxide reduction potential. This work highlights the often-underappreciated role that through-space electrostatics has in governing redox behaviour and provides a simple tool for tuning the oxidation behaviour of nitroxide radicals.

6.5 Modelling Nitroxide Mediated Polymerisations

Nitroxide mediated polymerization (NMP) was the first successful technique for controlled radical polymerization.[165] Full details of this process and its achievements are outlined in Chapter 7; for the present purposes it is important to note that the key to control rests with: (a) tuning the equilibrium constant for alkoxyamine dissociation to sit within an ideal range whereby there are enough propagating radicals released to sustain a polymerization but not enough for significant chain termination; (b) minimising other chain stopping side reactions.

Computational chemistry can assist with both aspects of this design problem and this is illustrated with the case studies outlined below.

6.5.1 Methodology

The computational methods used to study NMP are similar to those used for redox processes: high-level single reference methods such as G3(MP2)-RAD with appropriate solvation corrections. An example showing agreement of theory and experiment is provided in Figure 6.19, where theory is obtained using an ONIOM correction to G3(MP2)-RAD and solvent is modelled using the PCM-UAKS continuum model.[166] In this case the Gibbs free energies of reaction agree to within a mean absolute deviation of 4.5 kJ mol^{-1}. The kinetics of most of the side reactions in NMP are likewise well described by the same methodology; however, the kinetics of the σ-bond dissociation are, as described in section 6.2.1, a multireference problem. Fortunately modelling the kinetics of alkoxyamine bond dissociation are important for predicting the outcome of an NMP process because the reverse reaction is essentially barrierless and hence the barrier for the forward process is dominated by the thermodynamics.[167]

INSERT FIGURE 6.19

6.5.2 Selected Applications

Linear-Free Energy Relationships for Modelling Structure-Reactivity Trends in Controlled Radical Polymerization Macromolecules.[166, 168, 169] A series of theoretical studies used computational chemistry to develop simple equations for predicting the bond dissociation Gibbs free energy (BDFE) and hence equilibrium constant in nitroxide mediated polymerization as a function of the leaving group and nitroxide. Key to this work was the identification of appropriate descriptors for the steric, resonance and polar properties of the nitroxide and alkyl radical, and statistical analysis to assess which of these factors were necessary to describe the bond energies. Within a series of alkoxyamines, it was found that the equilibrium constant was well described by the equation[166]

$$\log (K_{eq}) = -0.10IP - 0.177RSE - 0.130RSE_{nxd} + 38.3 \qquad (21)$$

In this equation, IP is the vertical ionization potential of the alkyl radical, RSE is the standard radical stabilization energy the alkyl radical, while RSE_{nxd} is a new descriptor for the nitroxide radical, related to the standard radical stabilization energy, but reflecting in this case the flexibility of the nitroxide to the geometric changes associated with formation of an alkoxyamine. In a follow-up study, the linear free energy relationship was expanded to cover multiple types of controlled radical polymerization. The resulting relationship obtained was[168]

$$BDFE[RX] = 20.8\,\theta[R] - 9.73\,IP[R] - 1.10\,RSE[R] + 192\,\theta[X] + 57.4\,EA[X] - 62.0\,Resonance[X] - 250 \qquad (22)$$

where the steric descriptors θ[R] and θ[X] are measured as Tolman's cone angle of Cl-R and CH_3-X respectively, the polar descriptors IP[R] and EA[X] are the (gas-phase) ionization energy of R• and electron affinity of X• respectively, and the radical stability or resonance descriptors RSE[R] and Resonance[X] are measured as the standard radical stabilization energy for R• and the inverse HOMO-LUMO energy gap for X•. Apart from providing a predictive relationship for the bond energy (and hence equilibrium constant for the controlling equilibrium), the

analysis of the descriptor values allows for a comparison of the relative importance of polar, steric and resonance effects in NMP versus atom transfer radical polymerization (ATRP) and reversible addition fragmentation chain transfer (RAFT) (Figure 6.20). From Figure 6.20 it is clear that steric effects are relatively consistent across the different processes, while polar effects are important for ATRP and RAFT, and resonance effects are important for NMP and RAFT. This in turn gives some guidance as to not only what control agent might be important for a particular type of polymer, but what controlled radical polymerization process itself might be necessary to target the right equilibrium constant.

INSERT FIGURE 6.20

Which Side-Reactions Compromise Nitroxide Mediated Polymerization?[170] In this work, a combination of quantum chemistry and kinetic modelling (using the software PREDICI) was used to identify the key side reactions in NMP and study how they varied for different combinations of NMP agents (specifically TEMPO, SG1 and DPAIO) and monomer (styrene, methyl acrylate and methyl methacrylate). A variety of side reactions had been proposed to interfere with NMP (Figure 6.21); through first principles modelling, the study was able to show that the main one was an intramolecular alkoxyamine decomposition (often referred to as 'disproportionation') via a Cope-type elimination, which was kinetically significant for TEMPO- and SG1-mediated polymerizations of MMA, and not significant for the other systems. The β-scission process was also found to be problematic for propagating radicals bearing an abstractable hydrogen. Interestingly, it was also found that, due to penultimate unit effects, the decomposition of alkoxyamines can occur via principally different mechanisms between the unimeric and polymeric species.

INSERT FIGURE 6.21

Computational Design of pH-Switchable Control Agents for Nitroxide Mediated Polymerization[155, 171-174] One of the disadvantages of nitroxide mediated polymerization is the relatively high temperatures needed for sufficient alkoxyamine dissociation. Not only does this render polymerization susceptible to side reactions, as seen above, but it also precludes alkoxyamines as a convenient source of carbon-centred radicals in natural product synthesis. Thus, if one could trigger alkoxyamine decomposition under mild conditions in a controlled manner this would be very attractive. One approach is using light and this is outlined below; another is using electrostatic effects. The basic principle behind this latter approach is to take advantage of the dipole associated with the N-O• functionality:

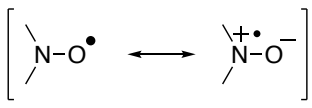

(23)

Thus a remote negative charge the nitrogen side of the nitroxide should stabilize this dipole and in doing stabilize the radical. Initial computational and experimental studies showed that indeed deprotonation of the carboxylic acid group in 4-carboxy-TEMPO lowered the gas-phase bond dissociation energies of its corresponding alkoxyamines by around 20 kJ mol^{-1}, irrespective of the leaving group.[171, 172] Follow up experimental studies in dichloromethane showed that this "pH-switch" decreased ca. 8.5 kJ mol^{-1} due to the increased dielectric constant of the reaction medium and associated decrease in the electrostatic interactions.[174]

At that level, while significant, the pH-switch was not large enough to allow 4-carboxy-TEMPO to facilitate NMP at room temperature.[173] Computational studies were thus undertaken to test other nitroxides, known and novel, to see if any would be suitable for room temperature NMP when charged and would be stable when neutral.[173] Design principles used in choosing the test set included synthetic accessibility, increasing the inherent stability of the nitroxide when uncharged, and placing the charge closer to the nitroxide (but without conjugation). Among the successful designs was a carboxy-TIPNO derivative which is indeed predicted to toggle between stability and radical release at room temperature (Figure 6.22). In this study, computational chemistry provided the initial insights behind electrostatic stabilization and its dependence on chemical structure,[171, 172] and subsequently allowed for a large number of molecules to be screened prior to undertaking laborious synthetic work.[173]

INSERT FIGURE 6.22

6.5 Studying Photoactive Nitroxides

Photoactive nitroxides remain an active area of interest, with potential uses as sensors, probes, and as nitroxide-mediated polymerization agents that can be activated under mild conditions.[175-177] Despite the reasonable amount of literature on photoactive nitroxides, and the well-established quenching of fluorescence upon formation of the nitroxide radical species, there is limited literature on exploring their excited states with computational methods.[178] Photoactive nitroxides do, however, exhibit several properties that can guide our approach to how we might explore their excited states. In this section, the different properties, how these properties can lead to different types of reactivity, and how we can model them, will be described.

6.6.1 Methodological Aspects

UV-Vis Spectra. Nitroxides like, for example, TEMPO exhibit thermal reactivity in which a stable nitroxide radical is formed, however its σ-bond framework does not lend itself to photoactivity. A widely used approach to increasing light absorption is to introduce highly conjugated chromophore substituents (Figure 6.23).[179-181] These extended π-systems introduce relatively low energy, bright $\pi\pi^*$ excited states as well as, provided nitrogen and/or oxygen are present, potentially reactive, spectroscopically dark, $n\pi^*$ states. The increased size of the potential molecules of interest can, however, prevent the application of *ab initio* excited state methods like, for example, Equation-of-Motion Coupled Cluster (EOM-CCSD)[182] or Algebraic Diagrammatic Construction (ADC(*n*)) methods.[183] The extensive conjugation can also give rise to significant correlation effects, for example doubly excited states or multiple low-lying excited states. These states are often difficult, or in the case of doubly excited state impossible, to capture using single-determinant excited state methods, for example time-dependent density functional theory (TD-DFT),[184] or time-dependent Hartree-Fock (TD-HF).[185] Ideally, multireference methods (CASSCF, CASPT2)[186] would be employed, which would be capable of capturing the nature of each excited state and any correlation effects. As with most multireference calculations, however, issues will remain with respect to the size of the active space required to accurately model the excited states, as the significant scaling issues will quickly prevent large molecules/large active spaces from being computationally tractable.

INSERT FIGURE 6.23

Often, the first test of suitability for a particular method is to compute the vertical excitation energies and oscillator intensities for a molecule at its ground-state, equilibrium geometry. Comparison of the computed spectrum against its experimental counterpart serves as a benchmark against which the accuracy of the method can be determined, and can immediately provide insight into the nature of the excited states of interest. When using wavefunction excited state methods, for example EOM-CCSD or CASSCF, it is important to ensure a large enough basis set is employed, as such methods exhibit a significant dependence between the calculated vertical excitation energy and basis set.[187, 188] At a minimum, a triple-zeta basis set ought to be employed augmented, if possible, with diffuse functions so as to more accurately model the less tightly bound excited state electrons and charge-transfer states. TD-DFT is found to exhibit a smaller basis set dependence, however its accuracy will too benefit from using a large basis set, if possible.[187]

Excited-State Charge Transfer. The introduction of chromophores does not necessarily result in the desired photoreactivity. Sometimes, this can be attributed to the separation of the conjugated chromophore and the reactive species by the nitroxide σ-framework, and can result in orbital localization, which in turn gives rise to charge-transfer states (Figure 6.24). To fully model these states, any multireference calculations should include the orbitals on each of the moieties, however this can be difficult if the active space becomes too large. If wavefunction calculations are too expensive to run, it is often necessary to turn to TD-DFT, which is much cheaper. In order to assess the best DFT functional to employ for the best accuracy and performance it may be necessary to consult existing benchmarking literature,[189] which can provide information about functional accuracy relative to the type of property being investigated. An important issue with TD-DFT is, however, its well documented failure when attempting to describe charge-transfer states, which precludes the use of traditional, uncorrected functionals (for example BLYP, B3LYP, or SVWN).[190] It is necessary instead to employ long-range corrected functionals; for example, LC-ωHPBE or ωB97X-D.[191] These functionals include parameters that mitigate self-interaction error in DFT and TD-DFT, and should correctly predict the $1/R$ asymptotic interaction between the localised charges of the charge-transfer states.

INSERT FIGURE 6.24

Non-Adiabatic Excited State Behaviour. Finally, upon excitation it is possible for the nitroxide molecule to undergo complex internal transfer processes like, for example, intersystem crossing (ISC) between different spin states to surfaces that may be highly reactive.[192] An example could be naphthalene tempo, which can be used as a photonitroxide mediated polymerisation agent.[179] Exciting the molecule could result in efficient ISC to a triplet surface; with the electrons unpaired, it is now easier to form the required reactive radical species.

The phenomena that give rise to efficient population of reactive states, for example conical intersections, can be difficult to model with single-determinant methods; the convergence of two excited state wavefunctions makes the corresponding regions of molecular geometry inherently multideterminant, and are best captured with multireference methods such as CASSCF and CASPT2. As mentioned earlier, however, if such methods are inappropriate for a given system it is often necessary to turn again to TD-DFT. Unfortunately, TD-DFT is unable to correctly describe the $3N$-8 dimensionality (where N is the number of atoms) of conical intersections.[193] Despite this, recent work suggests that CAM-B3LYP, M06-2X, and BH&HLYP

are capable of qualitatively reproducing the geometries at which conical intersections are found.[194] As well as this, M06-2X and BMK are two functionals found to best reproduce singlet-triplet gaps of the excited states of a range of organic molecules,[19] suggesting that the M06-2X functional at least should be applicable to nitroxide excited states and capable of capturing key aspects of nitroxide photoreactivity.

6.6.2 Selected Applications

Case Study: Theoretical Study of the Photochemical Initiation in Nitroxide-Mediated Photopolymerization.[178] In their 2014 paper, Huix-Rotllant *et al.*[178] employed computational methods to explore the photoinitiation mechanism of nitroxide mediated photopolymerisation. The molecule of interest, shown in Figure 6.25, is expected to exhibit several of the photochemical features described above; charge-transfer from the acetophenone to the *tert*-butyl moieties, and excited states of different symmetries, i.e. $\pi\pi^*$ and $n\pi^*$ states originating from the nitrogen and acyl oxygen groups. It is therefore important to select a method capable of at least qualitatively capturing potential states of interest. To that end, Huix-Rotllant *et al.*[178] used two methods, (unrestricted) DFT and the second-order extended multireference quasi-degenerate perturbation theory (XMCQDPT2),[195] to give a balanced description of the most likely photochemical processes taking place. The benefit of this approach is the bulk of the computational work can be performed with relatively cheap DFT, and (qualitative) accuracy is ensured by comparison with multireference methods. The active space employed for the multireference calculations contained the π/π^* and σ/σ^* of interest.

INSERT 6.25

The study examined the change in several properties; bond dissociation energies, ground- and excited-state equilibrium geometries, and their respective N-O and C-O bond lengths. The study was able to identify the key steps taking place in the photochemical dissociation reaction:

1. Absorption of photon and excitation to $n_O\pi^*$ state, localised on acetophenone moiety
2. Singlet-triplet intersystem crossing, localised still on acetophenone
3. Triplet energy delocalisation across alkoxyamine moiety
4. Bond dissociation of three bonds; $\sigma_{\text{O-C}}$ (desirable), and $\sigma_{\text{N-O}}$ and $\sigma_{\text{N-C}}$

6.6.3 Concluding remarks.

To conclude, due to their size and complicated photochemical processes, photoactive alkoxyamines present a challenge to current excited state computational methods. However, appropriate application of single- and multi-determinant methods should allow for a reliable, qualitative description of their key features. Single-determinant, “black-box” methods should either be correlated wavefunction methods (if possible), or TD-DFT using long-range corrected functionals with some portion of exact exchange. If necessary multireference

methods can also be employed, with active spaces consisting of relevant π-, σ-, and n-orbitals.

6.7 Further Applications

The applications of computational chemistry described in this Chapter are by no means exhaustive. For instance, computational chemistry has played an important in clarifying the mechanism of the Denisov cycle by which hindered amine light stabilizers protect polymers from oxidative damage,[196, 197] and identified a number of key side reactions in this process.[198, 199] These calculations were carried out using high-level single reference procedures, analogous to those used in studies of nitroxide mediated polymerization similar procedures. More recently, computational chemistry supported by experiment has been used to study the oxidative cleavage of alkoxyamines to produce nitroxide radicals and carbocations, both directly and promoted via S_N2 reactions with nucleophiles.[151, 152, 155] These studies used analogous procedures to those used in studies of nitroxide redox chemistry. On the basis of the mechanistic understanding provided by computational chemistry, a new *in situ* methylation procedure was designed and experimentally demonstrated.[200] This procedure, involving the bench and air stable TEMPO-Me reagent, offers major advantages over existing procedures which typically involve reagents with acute toxicity and high volatility. These are just some of the applications of quantum chemistry in studying nitroxide radical chemistry.

As seen in this chapter, the computational methods for studying nitroxides are many and various and the different types of system and property raise distinct methodological challenges. For instance, high spin systems and many excited states are invariably multi-reference in nature, redox potentials and bond energies while single reference usually require high levels of theory, moreover solvation effects are a potentially large source of error in redox systems, while EPR properties have their set of methods and require accurate treatments of core electrons, normally un-necessary in other systems. Nonetheless, in all cases, provided appropriated precautions are taken, methods exist to make chemically useful predictions.

Acknowledgments

MLC gratefully acknowledges support from the Australian Research Council (ARC) Centre of Excellence for Electromaterials Science and an ARC Laureate Fellowship.

References and Notes

1. S. Sanvito, *Chemical Society Reviews*, 2011, **40**, 3336-3355.
2. T. Sugawara and M. M. Matsushita, *Journal of Materials Chemistry*, 2009, **19**, 1738-1753.
3. I. Ratera and J. Veciana, *Chemical Society Reviews*, 2012, **41**, 303-349.
4. A. J. Wingate and B. W. Boudouris, *Journal of Polymer Science Part A: Polymer Chemistry*, 2016, **54**, 1875-1894.
5. M. Abe, *Chemical Reviews*, 2013, **113**, 7011-7088.
6. A. Szabo and N. Ostlund, *Modern Quantum Chemistry: Introduction to Advanced Electronic Structure Theory*, Dover Publications, 1996.

7. F. Jensen, *Introduction to Computational Chemistry*, John Wiley \&\#38; Sons, Inc., 2006.
8. A. J. Cohen, P. Mori-Sánchez and W. Yang, *Chemical Reviews*, 2012, **112**, 289-320.
9. D. K. W. Mok, R. Neumann and N. C. Handy, *The Journal of Physical Chemistry*, 1996, **100**, 6225-6230.
10. C. J. Cramer:, *Essentials of Computational Chemistry: Theories and Models*, Wiley, New York, 2002.
11. P. G. Szalay, T. Müller, G. Gidofalvi, H. Lischka and R. Shepard, *Chemical Reviews*, 2012, **112**, 108-181.
12. V. Veryazov, P. Å. Malmqvist and B. O. Roos, *International Journal of Quantum Chemistry*, 2011, **111**, 3329-3338.
13. R. Dawes and S. A. Ndengué, *International Reviews in Physical Chemistry*, 2016, **35**, 441-478.
14. F. Aiga, *The Journal of Physical Chemistry A*, 2012, **116**, 663-669.
15. F. Krausbeck, D. Mendive-Tapia, A. J. W. Thom and M. J. Bearpark, *Computational and Theoretical Chemistry*, 2014, **1040-1041**, 14-19.
16. K. Hirao, ed., *Recent Advances in Multireference Methods*, WORLD SCIENTIFIC, 1999.
17. H. J. Werner and P. J. Knowles, *The Journal of Chemical Physics*, 1985, **82**, 5053-5063.
18. R. J. Buenker and S. D. Peyerimhoff, *Theoretica chimica acta*, 1974, **35**, 33-58.
19. J. Miralles, O. Castell, R. Caballol and J.-P. Malrieu, *Chemical Physics*, 1993, **172**, 33-43.
20. V. M. García, M. Reguero and R. Caballol, *Theoretical Chemistry Accounts*, 1997, **98**, 50-56.
21. V. M. García, O. Castell, R. Caballol and J. P. Malrieu, *Chemical Physics Letters*, 1995, **238**, 222-229.
22. J. Finley, P.-Å. Malmqvist, B. O. Roos and L. Serrano-Andrés, *Chemical Physics Letters*, 1998, **288**, 299-306.
23. P. Celani and H.-J. Werner, *The Journal of Chemical Physics*, 2000, **112**, 5546-5557.
24. C. Li and F. A. Evangelista, *The Journal of Chemical Physics*, 2016, **144**, 164114.
25. D. I. Lyakh, M. Musiał, V. F. Lotrich and R. J. Bartlett, *Chemical Reviews*, 2012, **112**, 182-243.
26. H.-J. Werner, *Molecular Physics*, 1996, **89**, 645-661.
27. J. P. Malrieu, R. Caballol, C. J. Calzado, C. de Graaf and N. Guihéry, *Chemical Reviews*, 2014, **114**, 429-492.
28. P. Pulay, *International Journal of Quantum Chemistry*, 2011, **111**, 3273-3279.
29. J. P. Zobel, J. J. Nogueira and L. González, *Chemical science*, 2017, **8**, 1482-1499.
30. C. Camacho, H. A. Witek and S. Yamamoto, *Journal of Computational Chemistry*, 2009, **30**, 468-478.
31. I. Schapiro, K. Sivalingam and F. Neese, *Journal of Chemical Theory and Computation*, 2013, **9**, 3567-3580.
32. C. Angeli, M. Pastore and R. Cimiraglia, *Theoretical Chemistry Accounts*, 2007, **117**, 743-754.
33. S. Tolstikov, E. Tretyakov, S. Fokin, E. Suturina, G. Romanenko, A. Bogomyakov, D. Stass, A. Maryasov, M. Fedin, N. Gritsan and V. Ovcharenko, *Chemistry – A European Journal*, 2014, **20**, 2793-2803.
34. V. Barone, C. Boilleau, I. Cacelli, A. Ferretti, S. Monti and G. Prampolini, *Journal of Chemical Theory and Computation*, 2013, **9**, 300-307.

35. V. Barone, C. Boilleau, I. Cacelli, A. Ferretti and G. Prampolini, *Journal of Chemical Theory and Computation*, 2013, **9**, 1958-1963.
36. V. Barone, I. Cacelli, P. Cimino, A. Ferretti, S. Monti and G. Prampolini, *The Journal of Physical Chemistry A*, 2009, **113**, 15150-15155.
37. V. Barone, I. Cacelli, A. Ferretti and M. Girlanda, *The Journal of Chemical Physics*, 2008, **128**, 174303.
38. V. Barone, I. Cacelli, A. Ferretti, S. Monti and G. Prampolini, *Physical Chemistry Chemical Physics*, 2011, **13**, 4709-4714.
39. V. Barone, I. Cacelli, A. Ferretti, S. Monti and G. Prampolini, *Journal of Chemical Theory and Computation*, 2011, **7**, 699-706.
40. V. Barone, I. Cacelli, A. Ferretti and G. Prampolini, *Physical Chemistry Chemical Physics*, 2009, **11**, 3854-3860.
41. V. Barone, I. Cacelli and A. Ferretti, *Physical Chemistry Chemical Physics*, 2018, **20**, 18547-18555.
42. C. J. Calzado, C. Angeli, C. de Graaf and R. Caballol, *Theoretical Chemistry Accounts*, 2011, **128**, 505-519.
43. G. M. J. Barca, A. T. B. Gilbert and P. M. W. Gill, *Journal of Chemical Theory and Computation*, 2018, **14**, 1501-1509.
44. L. Noodleman, C. Y. Peng, D. A. Case and J. M. Mouesca, *Coordination Chemistry Reviews*, 1995, **144**, 199-244.
45. L. Noodleman, *The Journal of Chemical Physics*, 1981, **74**, 5737-5743.
46. K. Yamaguchi, Y. Takahara and T. Fueno, Dordrecht, 1986.
47. K. Yamaguchi, Y. Takahara, T. Fueno and K. N. Houk, *Theoretica chimica acta*, 1988, **73**, 337-364.
48. A. S. Menon and L. Radom, *The Journal of Physical Chemistry A*, 2008, **112**, 13225-13230.
49. K. Raghavachari and J. B. Anderson, *The Journal of Physical Chemistry*, 1996, **100**, 12960-12973.
50. Y. Kitagawa, T. Saito and K. Yamaguchi, 2018, DOI: 10.5772/intechopen.75726.
51. K. C. Ko, D. Cho and J. Y. Lee, *The Journal of Physical Chemistry A*, 2012, **116**, 6837-6844.
52. K. C. Ko, D. Cho and J. Y. Lee, *The Journal of Physical Chemistry A*, 2013, **117**, 3561-3568.
53. D. Cho, K. C. Ko and J. Y. Lee, *The Journal of Physical Chemistry A*, 2014, **118**, 5112-5121.
54. D. Cho, K. C. Ko and J. Y. Lee, *International Journal of Quantum Chemistry*, 2016, **116**, 578-597.
55. M. E. Ali and S. N. Datta, *The Journal of Physical Chemistry A*, 2006, **110**, 2776-2784.
56. M. E. Ali and S. N. Datta, *The Journal of Physical Chemistry A*, 2006, **110**, 10525-10527.
57. E. I. Izgorodina, D. R. B. Brittain, J. L. Hodgson, E. H. Krenske, C. Y. Lin, M. Namazian and M. L. Coote, *J. Phys. Chem. A*, 2007, **111**, 10754–10768.
58. D. Reta Mañeru, A. K. Pal, I. d. P. R. Moreira, S. N. Datta and F. Illas, *Journal of Chemical Theory and Computation*, 2014, **10**, 335-345.
59. A. I. Krylov, *Chemical Physics Letters*, 2001, **338**, 375-384.
60. A. I. Krylov, *Chemical Physics Letters*, 2001, **350**, 522-530.
61. A. I. Krylov and C. D. Sherrill, *The Journal of Chemical Physics*, 2002, **116**, 3194-3203.

62. Y. Shao, M. Head-Gordon and A. I. Krylov, *The Journal of Chemical Physics*, 2003, **118**, 4807-4818.
63. L. V. Slipchenko and A. I. Krylov, *The Journal of Chemical Physics*, 2002, **117**, 4694-4708.
64. S. V. Levchenko and A. I. Krylov, *The Journal of Chemical Physics*, 2003, **120**, 175-185.
65. A. A. Golubeva, A. V. Nemukhin, S. J. Klippenstein, L. B. Harding and A. I. Krylov, *The Journal of Physical Chemistry A*, 2007, **111**, 13264-13271.
66. T. Tsuchimochi, *The Journal of Chemical Physics*, 2015, **143**, 144114.
67. J. Mato and M. S. Gordon, *Physical Chemistry Chemical Physics*, 2018, **20**, 2615-2626.
68. X. Zhang and J. M. Herbert, *The Journal of Chemical Physics*, 2015, **143**, 234107.
69. D. Casanova and M. Head-Gordon, *Physical Chemistry Chemical Physics*, 2009, **11**, 9779-9790.
70. F. Bell, P. M. Zimmerman, D. Casanova, M. Goldey and M. Head-Gordon, *Physical Chemistry Chemical Physics*, 2013, **15**, 358-366.
71. M. Song, X. Song and Y. Bu, *Physical Chemistry Chemical Physics*, 2018, **20**, 8099-8111.
72. Z. Rolik, L. Szegedy, I. Ladjánszki, B. Ladóczki and M. Kállay, *J. Chem. Phys.*, 2013, **139**, 094105.
73. S. Stoll and A. Schweiger, *Journal of Magnetic Resonance*, 2006, **178**, 42-55.
74. D. R. Duling, *Journal of Magnetic Resonance, Series B*, 1994, **104**, 105-110.
75. D. Wang and G. R. Hanson, *Journal of Magnetic Resonance, Series A*, 1995, **117**, 1-8.
76. G. R. Hanson, C. J. Noble and S. Benson, in *High Resolution EPR: Applications to Metalloenzymes and Metals in Medicine*, eds. L. Berliner and G. Hanson, Springer New York, New York, NY, 2009, DOI: 10.1007/978-0-387-84856-3_4, pp. 105-173.
77. K. Khairy, D. Budil and P. Fajer, *Journal of Magnetic Resonance*, 2006, **183**, 152-159.
78. D. J. Schneider and J. H. Freed, in *Spin Labeling: Theory and Applications*, eds. L. J. Berliner and J. Reuben, Springer US, Boston, MA, 1989, DOI: 10.1007/978-1-4613-0743-3_1, pp. 1-76.
79. L. Hermosilla, J. M. García de la Vega, C. Sieiro and P. Calle, *J. Chem. Theory Comput.*, 2011, **7**, 1169-1179.
80. A. Savitsky, M. Plato and K. Möbius, *Applied Magnetic Resonance*, 2009, **37**, 415.
81. T. Janoschka, N. Martin, U. Martin, C. Friebe, S. Morgenstern, H. Hiller, M. D. Hager and U. S. Schubert, *Nature*, 2015, **527**, 78.
82. H. Nishide and K. Oyaizu, *Science*, 2008, **319**, 737-738.
83. T. Suga, H. Ohshiro, S. Sugita, K. Oyaizu and H. Nishide, *Advanced Materials*, 2009, **21**, 1627-1630.
84. T. Janoschka, M. D. Hager and U. S. Schubert, *Advanced Materials*, 2012, **24**, 6397-6409.
85. K. Zhang, Y. Hu, L. Wang, J. Fan, M. J. Monteiro and Z. Jia, *Polymer Chemistry*, 2017, **8**, 1815-1823.
86. J. B. Gerken and S. S. Stahl, *ACS Central Science*, 2015, **1**, 234-243.
87. A. Badalyan and S. S. Stahl, *Nature*, 2016, **535**, 406.
88. M. Rafiee, K. C. Miles and S. S. Stahl, *Journal of the American Chemical Society*, 2015, **137**, 14751-14757.
89. Q. Cao, L. M. Dornan, L. Rogan, N. L. Hughes and M. J. Muldoon, *Chemical Communications*, 2014, **50**, 4524-4543.
90. M. Zhang, C. Chen, W. Ma and J. Zhao, *Angewandte Chemie International Edition*, 2008, **47**, 9730-9733.

91. Z. Zhang, P. Chen, T. N. Murakami, S. M. Zakeeruddin and M. Grätzel, *Advanced Functional Materials*, 2008, **18**, 341-346.
92. J. Min, J. Won, Y. S. Kang and S. Nagase, *Journal of Photochemistry and Photobiology A: Chemistry*, 2011, **219**, 148-153.
93. T. Murakami, F. Kato, K. Oyaizu and H. Nishide, *Journal of Photopolymer Science and Technology*, 2010, **23**, 353-355.
94. K. Fumiaki, H. Naoki, M. Takaya, O. Chie, O. Kenichi and N. Hiroyuki, *Chemistry Letters*, 2010, **39**, 464-465.
95. B. P. Soule, F. Hyodo, K.-i. Matsumoto, N. L. Simone, J. A. Cook, M. C. Krishna and J. B. Mitchell, *Free Radical Biology and Medicine*, 2007, **42**, 1632-1650.
96. T. OFFER, A. RUSSO and A. SAMUNI, *The FASEB Journal*, 2000, **14**, 1215-1223.
97. M. B. Lauber and S. S. Stahl, *ACS Catalysis*, 2013, **3**, 2612-2616.
98. S. D. Rychnovsky, R. Vaidyanathan, T. Beauchamp, R. Lin and P. J. Farmer, *The Journal of Organic Chemistry*, 1999, **64**, 6745-6749.
99. M. Saita, J. Kaneko, T. Sato, S.-s. Takahashi, S. Wada-Takahashi, R. Kawamata, T. Sakurai, M.-C.-i. Lee, N. Hamada, K. Kimoto and Y. Nagasaki, *Biomaterials*, 2016, **76**, 292-301.
100. C. Abe, Y. Uto, A. Kawasaki, C. Noguchi, R. Tanaka, T. Yoshitomi, Y. Nagasaki, Y. Endo and H. Hori, *Journal of Controlled Release*, 2014, **182**, 67-72.
101. M. C. Krishna, D. A. Grahame, A. Samuni, J. B. Mitchell and A. Russo, *Proceedings of the National Academy of Sciences*, 1992, **89**, 5537-5541.
102. Y. Kinoshita, K.-i. Yamada, T. Yamasaki, F. Mito, M. Yamato, N. Kosem, H. Deguchi, C. Shirahama, Y. Ito, K. Kitagawa, N. Okukado, K. Sakai and H. Utsumi, *Free Radical Biology and Medicine*, 2010, **49**, 1703-1709.
103. A. V. Marenich, J. Ho, M. L. Coote, C. J. Cramer and D. G. Truhlar, *Physical Chemistry Chemical Physics*, 2014, **16**, 15068-15106.
104. J. Ho, M. Coote, C. Cramer and D. Truhlar, in *Organic Electrochemistry: Revised and Expanded*, eds. O. Hammerich and B. Speiser, CRC Press, Taylor and Francis Group, 2015, DOI: 10.1201/b19122-8, pp. 229-259.
105. L. E. Roy, E. Jakubikova, M. G. Guthrie and E. R. Batista, *The Journal of Physical Chemistry A*, 2009, **113**, 6745-6750.
106. R. S. Berry, S. A. Rice and J. Ross, *Physical Chemistry, Second Edition*, Oxford University Press, New York, 2000.
107. C. G. Zoski, *Handbook of Electrochemistry*, Elsevier, Amsterdam, 2007.
108. C. Møller and M. S. Plesset, *Phys. Rev.*, 1934, **46**, 618-622.
109. M. Head-Gordon, J. A. Pople and M. J. Frisch, *Chem. Phys. Lett.*, 1988, **153**, 503-506.
110. J. A. Pople, J. S. Binkley and R. Seeger, *Int. J. Quantum Chem.*, 1976, **10**, 1-19.
111. R. Krishnan and J. A. Pople, *Int. J. Quantum Chem.*, 1978, **14**, 91-100.
112. P. J. Knowles, J. S. Andrews, R. D. Amos, N. C. Handy and J. A. Pople, *Chem. Phys. Lett.*, 1991, **186**, 130-136.
113. W. J. Lauderdale, J. F. Stanton, J. Gauss, J. D. Watts and R. J. Bartlett, *Chem. Phys. Lett.*, 1991, **187**, 21-28.
114. W. J. Lauderdale, J. F. Stanton, J. Gauss, J. D. Watts and R. J. Bartlett, *J. Chem. Phys.*, 1992, **97**, 6606-6620.
115. G. D. Purvis and R. J. Bartlett, *J. Chem. Phys.*, 1982, **76**, 1910-1918.
116. G. E. Scuseria, C. L. Janssen and H. F. Schaefer, *J. Chem. Phys.*, 1988, **89**, 7382-7387.
117. J. A. Pople, M. Head-Gordon and K. Raghavachari, *J. Chem. Phys.*, 1987, **87**, 5968-5975.

118. J. Gauss and D. Cremer, *Chem. Phys. Lett.*, 1988, **150**, 280-286.
119. E. A. Salter, G. W. Trucks and R. J. Bartlett, *J. Chem. Phys.*, 1989, **90**, 1752-1766.
120. A. Tajti, P. G. Szalay, A. G. Császár, M. Kállay, J. Gauss, E. F. Valeev, B. A. Flowers, J. Vázquez and J. F. Stanton, *J. Chem. Phys.*, 2004, **121**, 11599-11613.
121. A. Karton, E. Rabinovich, J. M. L. Martin and B. Ruscic, *J. Chem. Phys.*, 2006, **125**, 144108.
122. J. A. Pople, M. Head-Gordon, D. J. Fox, K. Raghavachari and L. A. Curtiss, *J. Chem. Phys.*, 1989, **90**, 5622-5629.
123. L. A. Curtiss, C. Jones, G. W. Trucks, K. Raghavachari and J. A. Pople, *J. Chem. Phys.*, 1990, **93**, 2537-2545.
124. L. A. Curtiss, K. Raghavachari, G. W. Trucks and J. A. Pople, *J. Chem. Phys.*, 1991, **94**, 7221-7230.
125. L. A. Curtiss, K. Raghavachari, P. C. Redfern, V. Rassolov and J. A. Pople, *J. Chem. Phys.*, 1998, **109**, 7764-7776.
126. L. A. Curtiss, P. C. Redfern and K. Raghavachari, *J. Chem. Phys.*, 2007, **126**, 084108.
127. D. J. Henry, M. B. Sullivan and L. Radom, *J. Chem. Phys.*, 2003, **118**, 4849-4860.
128. M. R. Nyden and G. A. Petersson, *J. Chem. Phys.*, 1981, **75**, 1843-1862.
129. G. A. Petersson, A. Bennett, T. G. Tensfeldt, M. A. Al-Laham, W. A. Shirley and J. Mantzaris, *J. Chem. Phys.*, 1988, **89**, 2193-2218.
130. G. A. Petersson and M. A. Al-Laham, *J. Chem. Phys.*, 1991, **94**, 6081-6090.
131. G. A. Petersson, T. G. Tensfeldt and J. A. Montgomery, *J. Chem. Phys.*, 1991, **94**, 6091-6101.
132. J. A. Montgomery, J. W. Ochterski and G. A. Petersson, *J. Chem. Phys.*, 1994, **101**, 5900-5909.
133. J. W. Ochterski, G. A. Petersson and J. A. Montgomery, *J. Chem. Phys.*, 1996, **104**, 2598-2619.
134. J. A. Montgomery, M. J. Frisch, J. W. Ochterski and G. A. Petersson, *J. Chem. Phys.*, 1999, **110**, 2822-2827.
135. J. A. Montgomery, M. J. Frisch, J. W. Ochterski and G. A. Petersson, *J. Chem. Phys.*, 2000, **112**, 6532-6542.
136. J. M. L. Martin and G. de Oliveira, *J. Chem. Phys.*, 1999, **111**, 1843-1856.
137. S. Parthiban and J. M. L. Martin, *J. Chem. Phys.*, 2001, **114**, 6014-6029.
138. A. D. Boese, M. Oren, O. Atasoylu, J. M. L. Martin, M. Kállay and J. Gauss, *J. Chem. Phys.*, 2004, **120**, 4129-4141.
139. D. Bednarczyk and J. Bednarczyk, *Physics Letters A*, 1978, **64**, 409-410.
140. P. Hohenberg and W. Kohn, *Phys. Rev.*, 1964, **136**, B864-B871.
141. W. Kohn and L. J. Sham, *Phys. Rev.*, 1965, **140**, A1133-A1138.
142. E. I. Izgorodina, M. L. Coote and L. Radom, *J. Phys. Chem. A*, 2005, **109**, 7558-7566.
143. J. L. Hodgson, M. Namazian, S. E. Bottle and M. L. Coote, *The Journal of Physical Chemistry A*, 2007, **111**, 13595-13605.
144. M. Isegawa, F. Neese and D. A. Pantazis, *Journal of Chemical Theory and Computation*, 2016, **12**, 2272-2284.
145. J. Ho, A. Klamt and M. L. Coote, *J. Phys. Chem. A*, 2010, **114**, 13442–13444.
146. J. Tomasi, *Theor. Chem. Acc.*, 2004, **112**, 184–203.
147. A. V. Marenich, J. Ho, M. L. Coote, C. J. Cramer and D. G. Truhlar, *Phys. Chem. Chem. Phys.*, 2014, **16**, 15068-15106.
148. J. Ho and M. L. Coote, *J. Chem. Theory Comput.*, 2009, **5**, 295-306.

149. J. R. Pliego Jr. and J. M. Riveros, *J. Phys. Chem. A*, 2001, **105**, 7241–7247.
150. A. V. Marenich, C. J. Cramer and D. G. Truhlar, *The Journal of Physical Chemistry B*, 2009, **113**, 6378-6396.
151. C. L. Hammill, B. B. Noble, P. L. Norcott, S. Ciampi and M. L. Coote, *The Journal of Physical Chemistry C*, 2019, **123**, 5273-5281.
152. B. B. Noble, P. L. Norcott, C. L. Hammill, S. Ciampi and M. L. Coote, *The Journal of Physical Chemistry C*, 2019, **123**, 10300-10305.
153. F. J. M. Rogers and M. L. Coote, *The Journal of Physical Chemistry C*, 2019, **123**, 20174-20180.
154. F. J. M. Rogers and M. L. Coote, *The Journal of Physical Chemistry C*, 2019, **123**, 10306-10310.
155. L. Zhang, E. Laborda, N. Darwish, B. B. Noble, J. H. Tyrell, S. Pluczyk, A. P. Le Brun, G. G. Wallace, J. Gonzalez, M. L. Coote and S. Ciampi, *Journal of the American Chemical Society*, 2018, **140**, 766-774.
156. L. Zhang, Y. B. Vogel, B. B. Noble, V. R. Gonçales, N. Darwish, A. L. Brun, J. J. Gooding, G. G. Wallace, M. L. Coote and S. Ciampi, *Journal of the American Chemical Society*, 2016, **138**, 9611-9619.
157. G. Gryn'ova, J. M. Barakat, J. P. Blinco, S. E. Bottle and M. L. Coote, *Chemistry – A European Journal*, 2012, **18**, 7582-7593.
158. F. Kato, A. Kikuchi, T. Okuyama, K. Oyaizu and H. Nishide, *Angewandte Chemie*, 2012, **124**, 10324-10327.
159. K. Zhang, B. B. Noble, A. C. Mater, M. J. Monteiro, M. L. Coote and Z. Jia, *Physical Chemistry Chemical Physics*, 2018, **20**, 2606-2614.
160. J. P. Blinco, J. L. Hodgson, B. J. Morrow, J. R. Walker, G. D. Will, M. L. Coote and S. E. Bottle, *The Journal of Organic Chemistry*, 2008, **73**, 6763-6771.
161. M. Kavala, R. Boča, L. Dlháň, V. Brezová, M. Breza, J. Kožíšek, M. Fronc, P. Herich, L. Švorc and P. Szolcsányi, *The Journal of Organic Chemistry*, 2013, **78**, 6558-6569.
162. K. Daze and F. Hof, in *Encyclopedia of Physical Organic Chemistry*, eds. Z. Wang, U. Wille and E. Juaristi, Wiley, 2016, DOI: 10.1002/9781118468586.epoc3001, pp. 1-51.
163. C. R. Martinez and B. L. Iverson, *Chemical Science*, 2012, **3**, 2191-2201.
164. A. S. Shetty, J. Zhang and J. S. Moore, *Journal of the American Chemical Society*, 1996, **118**, 1019-1027.
165. C. J. Hawker, A. W. Bosman and E. Harth, *Chem. Rev.*, 2001, **101**, 3661–3688.
166. J. L. Hodgson, C. Yeh Lin, M. L. Coote, S. R. A. Marque and K. Matyjaszewski, *Macromolecules*, 2010, **43**, 3728-3743.
167. J. L. Hodgson, L. B. Roskop, M. S. Gordon, C. Y. Lin and M. L. Coote, *The Journal of Physical Chemistry A*, 2010, **114**, 10458-10466.
168. C. Y. Lin, S. R. A. Marque, K. Matyjaszewski and M. L. Coote, *Macromolecules*, 2011, **44**, 7568-7583.
169. S. Marque, *The Journal of Organic Chemistry*, 2003, **68**, 7582-7590.
170. G. Gryn'ova, C. Y. Lin and M. L. Coote, *Polymer Chemistry*, 2013, **4**, 3744-3754.
171. G. Gryn'ova, D. L. Marshall, S. J. Blanksby and M. L. Coote, *Nature Chemistry*, 2013, **5**, 474.
172. G. Gryn'ova and M. L. Coote, *Journal of the American Chemical Society*, 2013, **135**, 15392-15403.
173. G. Gryn'ova, L. M. Smith and M. L. Coote, *Physical Chemistry Chemical Physics*, 2017, **19**, 22678-22683.

174. M. Klinska, L. M. Smith, G. Gryn'ova, M. G. Banwell and M. L. Coote, *Chemical Science*, 2015, **6**, 5623-5627.
175. J. P. Blinco, K. E. Fairfull-Smith, B. J. Morrow and S. E. Bottle, *Australian Journal of Chemistry*, 2011, **64**, 373-373.
176. M. Eing, B. T. Tuten, J. P. Blinco and C. Barner-Kowollik, *Chemistry - A European Journal*, 2018, **24**, 12246-12249.
177. K. A. Hansen and J. P. Blinco, *Polymer Chemistry*, 2018, **9**, 1479-1516.
178. M. Huix-Rotllant and N. Ferre, *Journal of Physical Chemistry A*, 2014, **118**, 4464-4470.
179. S. E. Bottle, J.-L. Clement, M. Fleige, E. M. Simpson, Y. Guillaneuf, K. E. Fairfull-Smith, D. Gigmes and J. P. Blinco, *RSC Adv.*, 2016, **6**, 80328-80333.
180. S. Coiai, E. Passaglia and F. Cicogna, *Polymer International*, 2019, **68**, 27-63.
181. Y. Guillaneuf, D. Bertin, D. Gigmes, D.-L. Versace, J. Lalevée and J.-P. Fouassier, *Macromolecules*, 2010, **43**, 2204-2212.
182. M. Caricato, *Journal of Chemical Theory and Computation*, 2012, **8**, 5081-5091.
183. A. Dreuw and M. Wormit, *Wiley Interdisciplinary Reviews: Computational Molecular Science*, 2015, **5**, 82-95.
184. R. Ahlrichs and R. Bauernschmitt, *Chemical Physics Letters*, 1996, **256**, 454-464.
185. M. A. Ball and A. D. McLachlan, *Molecular Physics*, 1964, **7**, 501-513.
186. V. Veryazov, P.-A. Malmqvist and B. O. Roos, *International Journal of Quantum Chemistry*, 2011, **111**, 3329-3338.
187. A. D. Laurent, A. Blondel and D. Jacquemin, *Theoretical Chemistry Accounts*, 2015, **134**, 1-11.
188. M. Schreiber, M. R. Silva-Junior, S. P. A. Sauer and W. Thiel, *Journal of Chemical Physics*, 2008, **128**.
189. A. D. Laurent and D. Jacquemin, *International Journal of Quantum Chemistry*, 2013, **113**, 2019-2039.
190. A. Dreuw and M. Head-Gordon, *Journal of the American Chemical Society*, 2004, **126**, 4007-4016.
191. Y. Jiang, Z. Hu, B. Zhou, C. Zhong, Z. Sun and H. Sun, *The Journal of Physical Chemistry C*, 2019, **123**, 5616-5625.
192. W. Domcke and D. R. Yarkony, *Annual Review of Physical Chemistry*, 2012, **63**, 325-352.
193. Y. Shu, K. A. Parker and D. G. Truhlar, *Journal of Physical Chemistry Letters*, 2017, **8**, 2107-2112.
194. M. Filatov, *Journal of Chemical Theory and Computation*, 2013, **9**, 4526-4541.
195. A. A. Granovsky, *Journal of Chemical Physics*, 2011, **134**.
196. G. Gryn'ova, K. U. Ingold and M. L. Coote, *Journal of the American Chemical Society*, 2012, **134**, 12979-12988.
197. J. L. Hodgson and M. L. Coote, *Macromolecules*, 2010, **43**, 4573-4583.
198. M. R. L. Paine, G. Gryn'ova, M. L. Coote, P. J. Barker and S. J. Blanksby, *Polymer Degradation and Stability*, 2014, **99**, 223-232.
199. D. L. Marshall, M. L. Christian, G. Gryn'ova, M. L. Coote, P. J. Barker and S. J. Blanksby, *Organic & Biomolecular Chemistry*, 2011, **9**, 4936-4947.
200. P. L. Norcott, C. L. Hammill, B. B. Noble, J. C. Robertson, A. Olding, A. C. Bissember and M. L. Coote, *Journal of the American Chemical Society*, 2019, DOI: 10.1021/jacs.9b08634.

Table 1. Relative aqueous oxidation (E_{ox}) and reduction (E_{red}) potentials for piperidine, pyrrolidine, azaphenalene [a] and isoindoline nitroxides. Data taken from Reference ref. [143]

Nitroxide	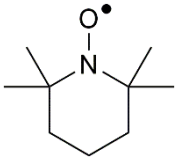	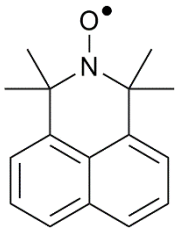	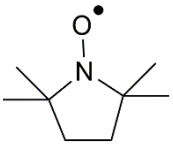	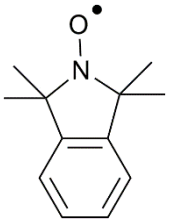
E_{red} (mV)	0.0	+146	−138	−22
E_{ox} (mV)	0.0	+267	+2	+240

[a] Data for the azaphenelene was subsequently corrected in Ref [157] and we show the corrected data here.

Figures and Captions

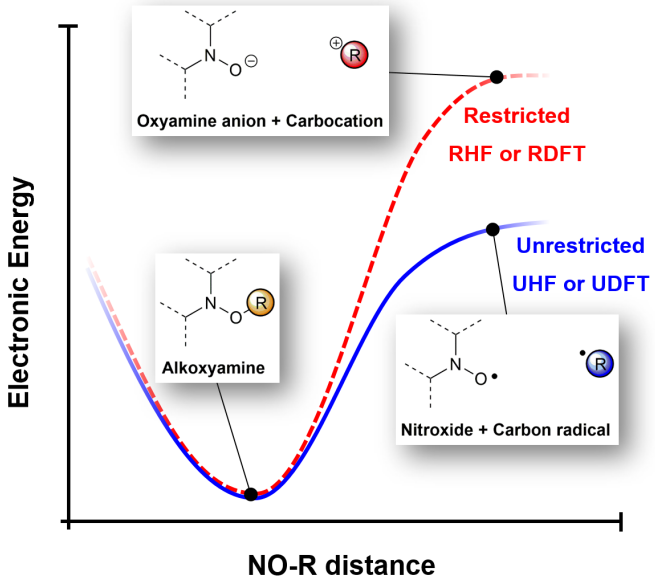

Figure 6.1 Idealised potential energy surfaces for NO-R bond dissociation. Restricted theory (RHF and correlated variants, RDFT) uses the same spatial components for both alpha and beta spin orbitals and consequently it cannot describe bond homolysis. In Unrestricted theory (UHF and correlated variants, UDFT) these spatial components are allowed to vary, which provides a better description of homolytic processes (albeit with the introduction spin contamination, see text).

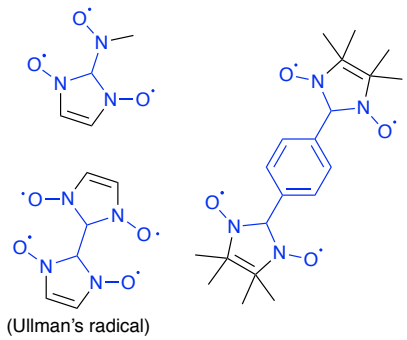

Figure 6.2. Test set in Ref [41]. Blue indicates the fragments, whose MOs are considered in the construction of the DDCI space.

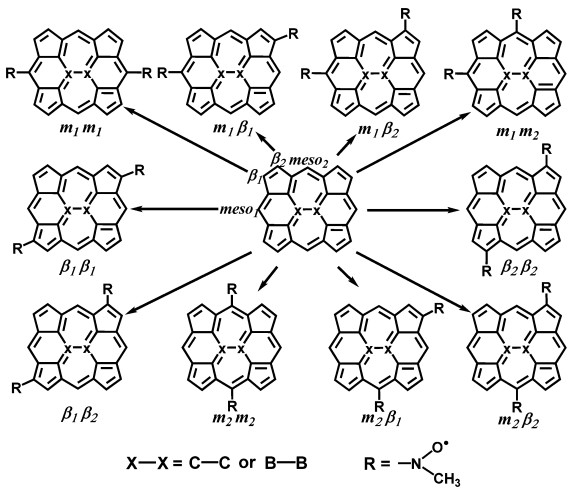

Figure 6.3 Test set of porphyrin bridged nitroxide diradicals in Ref [71]. Reproduced from Ref. [71] with permission from the PCCP Owner Societies.

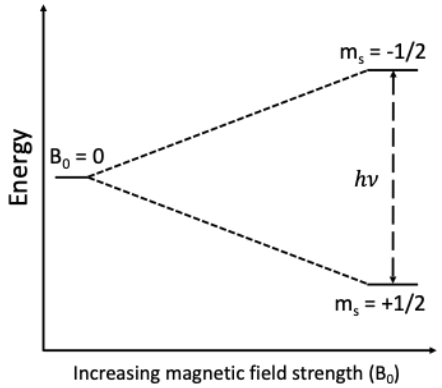

Figure 6.4 - Splitting in electron spin states observed upon introduction of a magnetic field

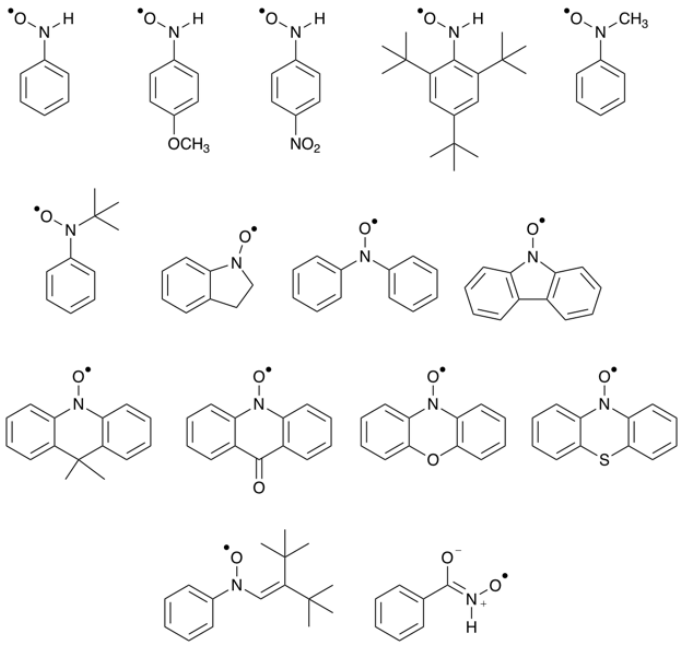

Figure 6.5 – Nitroxide radicals studied in ref [79]

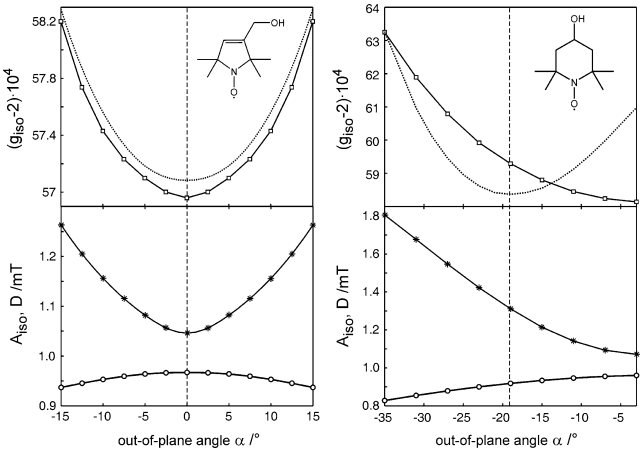

Figure 6.6. The calculated g_{iso} (open square), A_{iso} (asterisk) and D (open circle) values as a function of out- of-plane angle α for 3-hydroxymethyl-2,2,5,5- tetramethylpyrrolin-1-oxyl (left) and 4-hydroxy-2,2,6,6-tetramethylpiperidine-N-oxyl (right). The dotted line shows the relaxed energy profile, and the dashed line indicates the minimum energy angle. Reproduced directly from Ref [80].

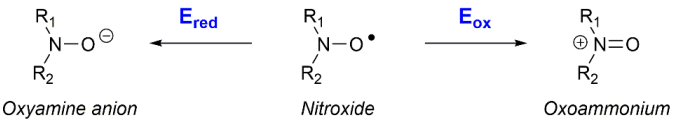

Figure 6.7. The oxidation and reduction of a nitroxide of the general form, $R_1R_2N{-}O^{\bullet}$.

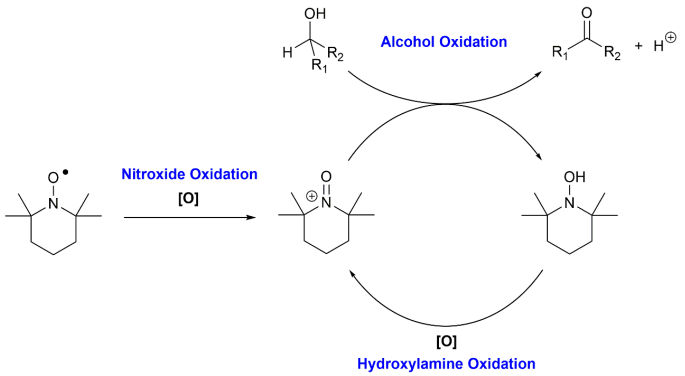

Figure 6.8. The nitroxide catalysed oxidation of an alcohol to a ketone in the presence of bulk stoichiometric oxidant [O].

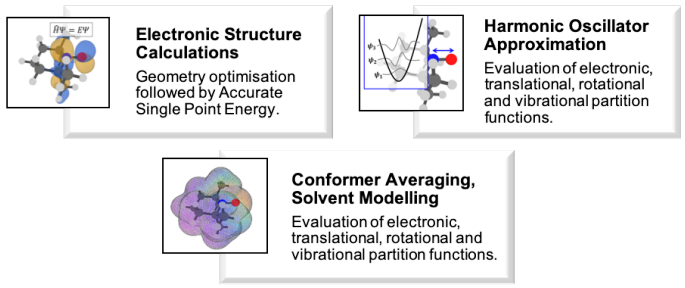

Figure 6.9. The three steps involved in the calculation of oxidation and reduction potentials.

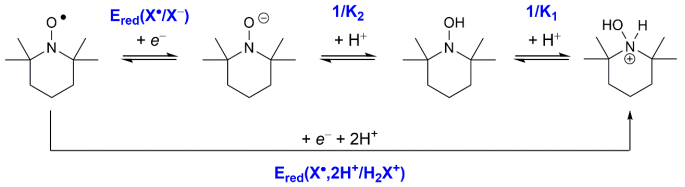

Figure 6.10. Chemical processes associated with the reduction of the TEMPO• radical in water.

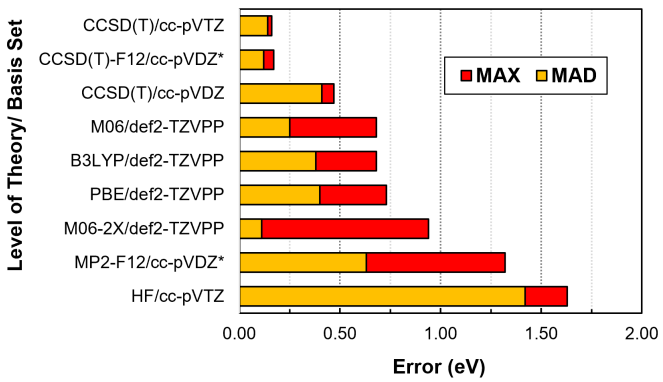

Figure 6.11. Mean Absolute Error (MAD) and Maximum Errors (MAX) in Adiabatic Ionization Energies for the 19 organic species in the Pantazis test set, taken from reference [144].*Indicates a F12 variant of the standard cc-pVDZ basis set was used.

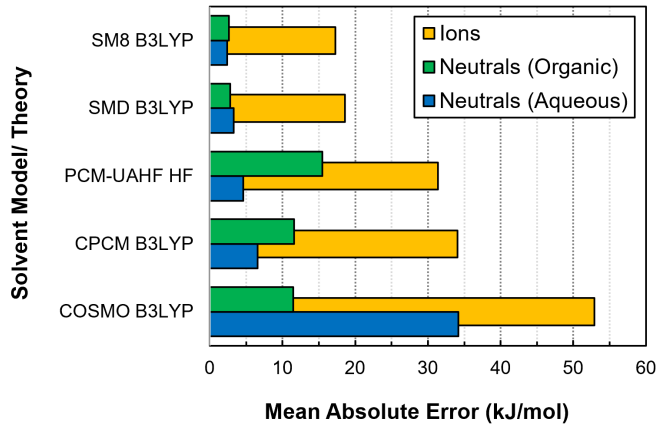

Figure 6.12. Typical errors for ionic and neutral species in popular continuum solvation models.

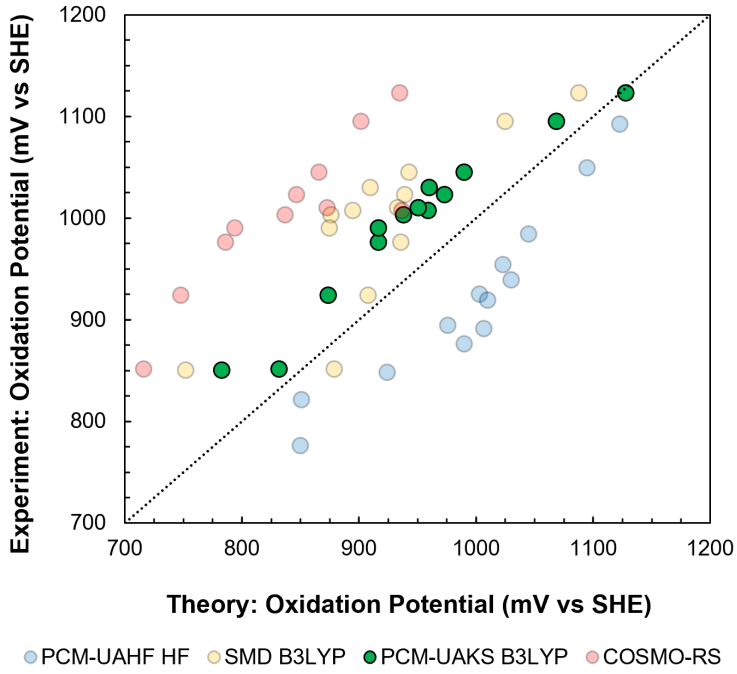

Figure 6.13. The performance of different solvent methodologies for the computational prediction of nitroxide oxidation potentials.

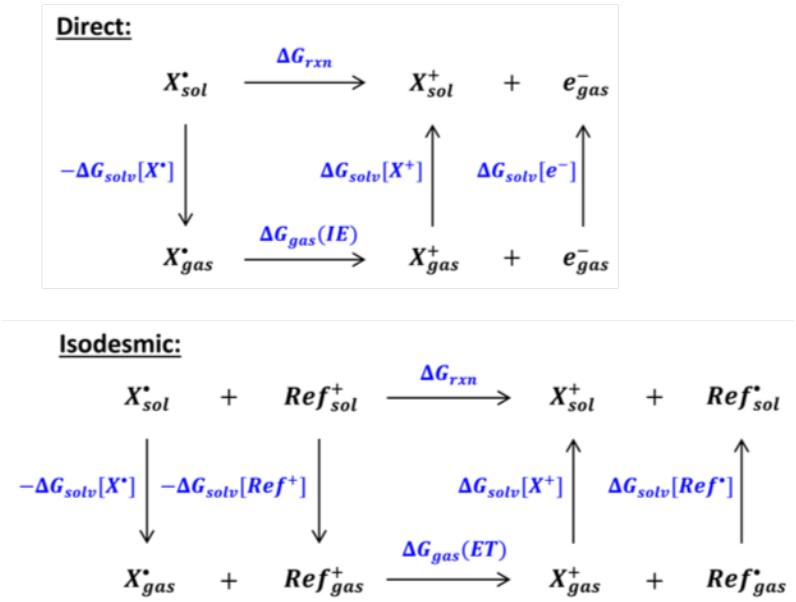

Figure 6.14. Direct vs Isodesmic Oxidation Potential Calculations.

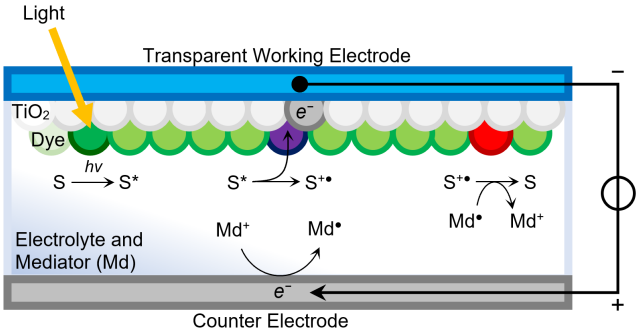

Figure 6.15 A simplified depiction of a Dye-Sensitised Solar Cell, showing the principal photoexcitation and electron transfer processes.

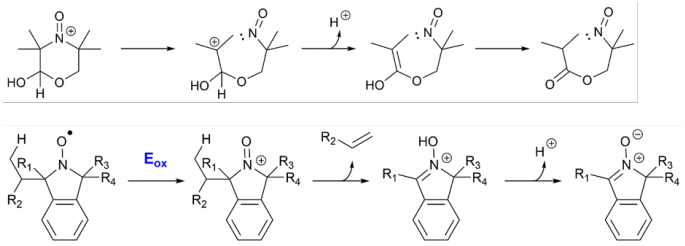

Figure 6.16. (Top) Proposed ring opening pathway of a hydroxyl substituted morpholine oxoammonium. The electrochemical oxidation of the corresponding nitroxide is nearly completely irreversible. (Bottom) The generation of isoindoline-derived nitrononeS via β−fragmentation from the corresponding oxoammonium (with loss of an alkene)

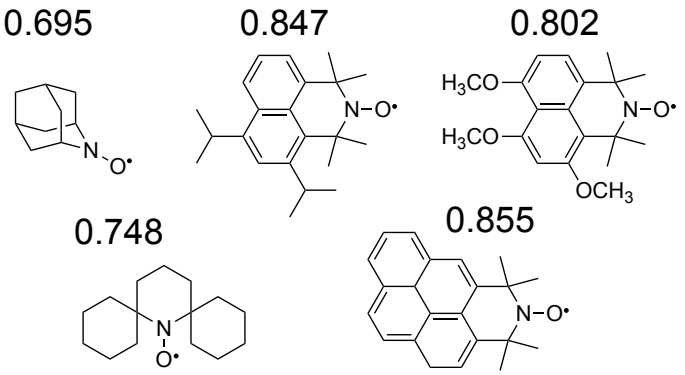

Figure 6.17. Proposed redox mediators showing computed potentials in V vs SHE. Figure taken directly from Ref [157].

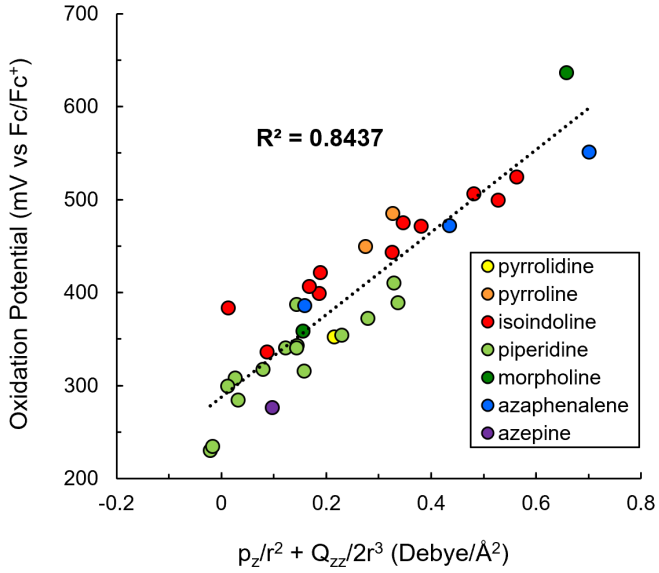

Figure 6.18. The generation of isoindoline-derived nitrononones via β−fragmentation from the corresponding oxoammonium (with loss of an alkene). Data taken from Ref [159]

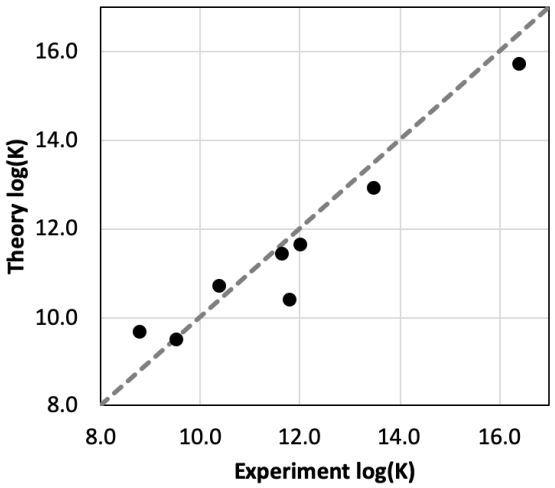

Figure 6.19. Comparison of quantum-chemical and experimental equilibrium constants for alkoxyamine dissociation. Theoretical calculations performed using an ONIOM approximation of G3(MP2)-RAD//B3-LYP/6-31G(d) in conjunction with PCM-UAKS solvation energies at the B3-LYP/6-31G(d) level. Data taken from Ref [166].

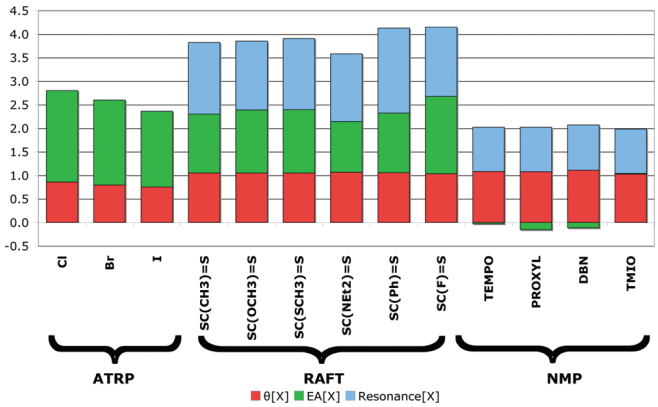

Figure 6.20 Values of each of the X-descriptors in dimensionless units (obtained by dividing each value by the average value for that descriptor across the full data set). Figure reproduced directly from Ref. [168].

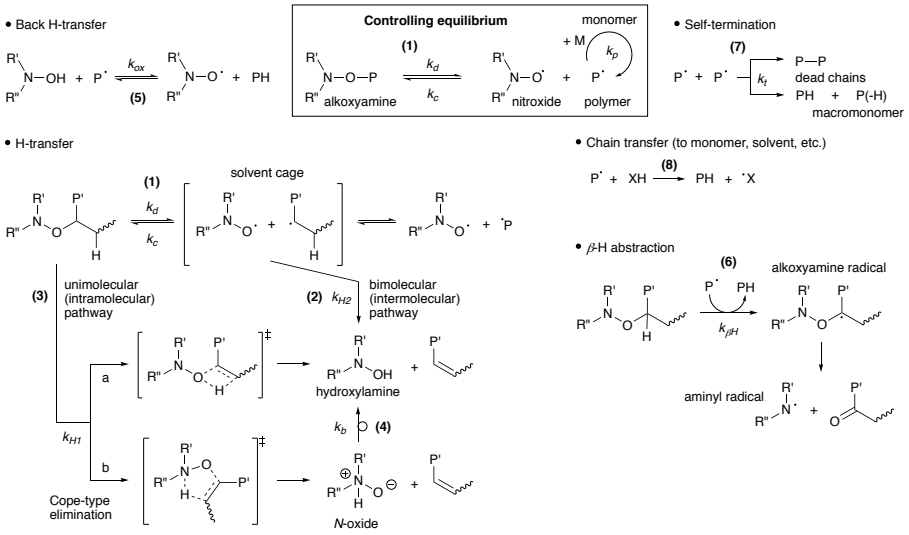

Figure 6.21 Nitroxide mediated polymerization and its competing side-reactions. Figure reproduced directly from Ref. [170].

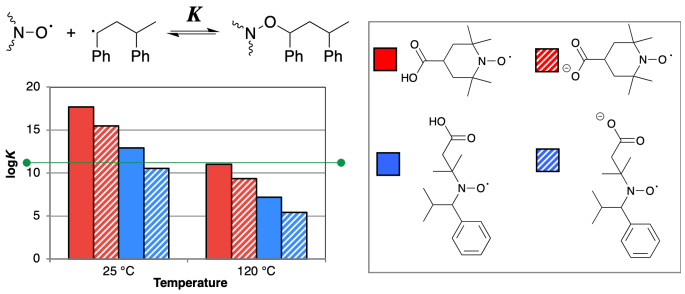

Figure 6.22 Change in equilibrium constant (in bulk styrene at 120°C and 25°C) upon deprotonation of 4-carboxy-TEMPO and a TIPNO derivative bearing a remote carboxylic acid group. The green line shows the equilibrium constant of neutral 4-carboxy-TEMPO, which functions well at 120°C and represents a target value for the deprotonated species at room temperature. Above this line the alkoxyamine is too stable to sustain a polymerization; below it too many radicals are released for control. Data taken from Ref. [173].

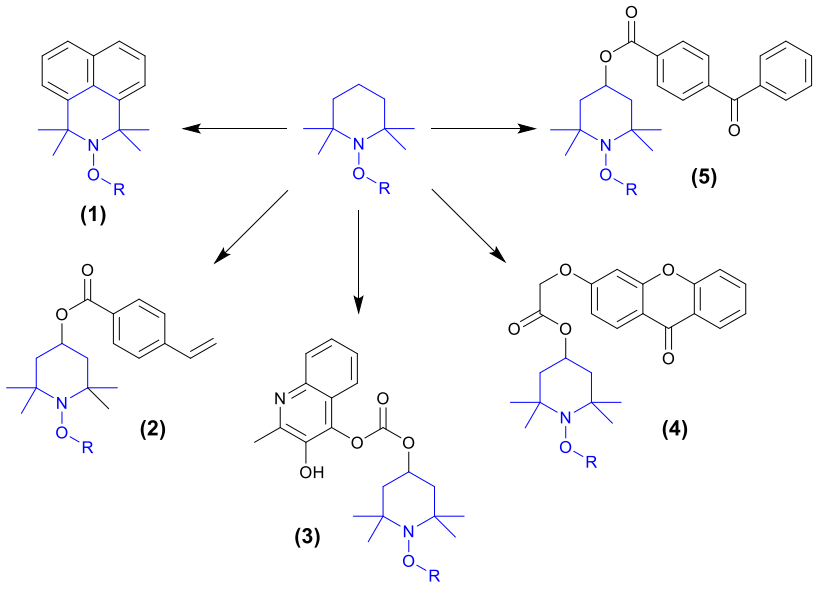

Figure 6.23 Examples of TEMPO-derived, photoactive nitroxide compounds, using naphthalene[179] **(1)**, benzoyloxy[180] **(2)**, quinoline[181] **(3)**, xanthenone[181] **(4)**, and diphenyl-methanone[181] **(5)** based chromophores.

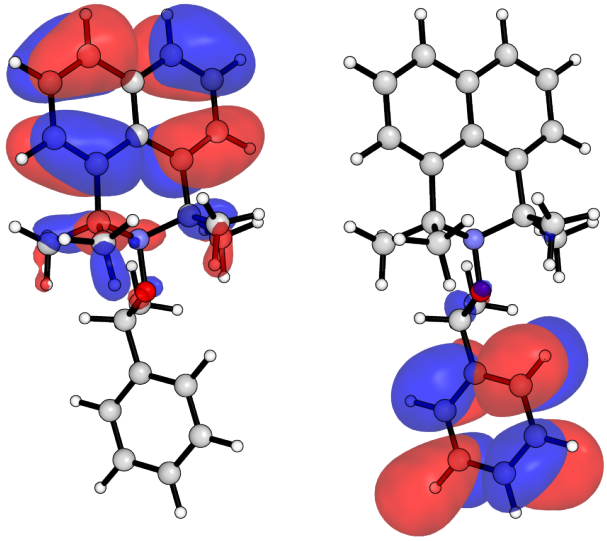

Figure 6.24. Orbital localization of π-system across the naphthalene moiety (left), and localization of π^*-system across the styrene moiety (right)

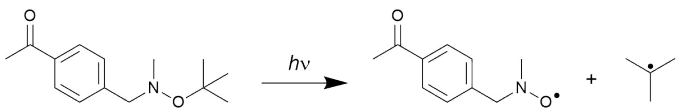

Figure 6.25. Photodissociation mechanism investigated by Huix-Rotllant *et al.* [178]